



Controls on Sediment Suspension, Flux, and Marsh Deposition near a Bay-Marsh Boundary

Melissa S. Duvall^{1,2} · Patricia L. Wiberg¹ · Matthew L. Kirwan³

Received: 5 July 2017 / Revised: 7 September 2018 / Accepted: 15 October 2018
© Coastal and Estuarine Research Federation 2018

Abstract

The sustainability of marshes adjacent to coastal bays is driven by the exchange of sediment across the marsh-bay boundary, where edge erosion commonly leads to lateral marsh loss and enhanced vertical accretion. The timing and patterns of sediment deposition on salt marshes adjacent to larger bodies of water such as coastal bays, however, differ from those on better-studied tidal creek marshes primarily owing to the importance of wind-waves. We combined field measurements and modeling to examine controls on suspended sediment concentrations and fluxes on a tidal flat (tidal range of 1.2 m) and rates of sediment deposition on the adjacent marsh at a site on the Eastern Shore of Virginia. Suspended sediment concentrations over tidal flats were strongly controlled by waves. Yet, storm winds sufficient to drive large resuspension events often coincided with peak tidal elevations that were too low to flood the marsh, which was oriented away from the wind directions most favorable for storm surge, thereby restricting storm-driven, episodic sediment delivery to the marsh. Winds also drove wide variability in the direction of surface currents near the marsh edge when water depths were high enough to flood the marsh. Nevertheless, our results show that sediment in the upper water column over the tidal flat was effectively transported across the marsh edge during flooding tides. A sediment deposition model developed to investigate the combined effects of vegetation and wave action on depositional patterns predicted that waves displace maximum deposition inland from the marsh edge, consistent with measured deposition at the study site. Marsh deposition was sensitive to inundation frequency as well as the concentration of sediment in water flooding the marsh, underscoring the importance of nontidal controls on water surface elevation, such as meteorological effects (e.g., storm surge) and sea level rise. Whereas short-term increases in marsh inundation enhance deposition, sea level rise that results in deeper average water depths over the tidal flats decreases deposition if marsh elevation is rising in step with sea level.

Keywords Suspended sediment concentrations · Sediment flux · Sediment deposition · Salt marsh · Shallow coastal bays · Storms · Sea-level rise

Communicated by Carl T. Friedrichs

Electronic supplementary material The online version of this article (<https://doi.org/10.1007/s12237-018-0478-4>) contains supplementary material, which is available to authorized users.

✉ Melissa S. Duvall
Melissa.duvall@duke.edu

- ¹ Department of Environmental Sciences, University of Virginia, Charlottesville, VA, USA
- ² Nicholas School of the Environment, Duke University Marine Laboratory, 135 Duke Marine Lab Road, Beaufort, NC 28516, USA
- ³ Virginia Institute of Marine Science, College of William & Mary, Gloucester Point, VA, USA

Introduction

As sea level rises, the persistence of intertidal salt marshes depends on their ability to maintain their elevation relative to sea level. The vertical position of the marsh platform with respect to sea level is determined by the rate of relative sea level rise (RSLR), organic matter accumulation, and mineral sediment deposition (Cahoon and Reed 1995). Threshold rates of RSLR that trigger marsh drowning depend strongly on the concentration of sediment suspended in the water flooding the marsh (Kirwan et al. 2010), a proxy for the sediment available to be deposited on the marsh surface.

The factors influencing sediment deposition on tidal creek marshes have been relatively well characterized (e.g., Leonard 1997; Christiansen et al. 2000; Friedrichs and Perry 2001; Temmerman et al. 2003; Fagherazzi et al. 2013; Ganju et al.

2015; Ensign and Currin 2017). In contrast, the factors affecting depositional processes at bay-marsh boundaries have received less attention. There are three main differences between tidal creek marshes and marshes bordering coastal bays. The most important is the presence of waves, which episodically increase bed shear stress (Fagherazzi and Wiberg 2009; Mariotti et al. 2010), resuspend sediment on adjacent tidal flats (Lawson et al. 2007; Carniello et al. 2012), and dissipate their energy either on the marsh edge scarp (Tonelli et al. 2010; Marani et al. 2011) or over the marsh platform as they encounter marsh vegetation (Möller et al. 1996, 1999, 2014). The second is that the lateral position of the bay-marsh boundary is inherently unstable, perpetually retreating or prograding (Mariotti and Fagherazzi 2013; Fagherazzi et al. 2013) in contrast to the often-stable location of tidal creek banks. Finally, the complex pattern of tidal and wind-driven flow on tidal flats and adjacent marsh surfaces is reflected by the wide variability in the net direction of suspended sediment flux over the tidal flats bordering a marsh. Characterizing the transport of sediment across these bay-marsh boundaries is important because erosion along bay edges is both a primary mechanism for lateral marsh loss (Fagherazzi 2013), and a source of sediment for sustaining vertical marsh accretion (Mariotti and Carr 2014).

A number of recent studies have focused on rates of lateral change in the position of marsh-bay boundaries (Marani et al. 2011; McLoughlin et al. 2015; Deaton et al. 2017), and the consequences of marsh edge retreat for the overall evolution of marsh-bay and marsh-bay-upland systems (Mariotti and Fagherazzi 2013; Kirwan et al. 2016). Few studies, however, have measured time series of currents, waves, tides and turbidity at a bay-marsh boundary, which is important for understanding and modeling sediment delivery to bay-fronted marshes and quantifying sediment budgets for marsh-bay systems. Studies that have measured some of these parameters near mudflat-salt marsh boundaries (Widdows et al. 2008; Pratolongo et al. 2010; Callaghan et al. 2010) have been in environments with a tidal range of 4 m or more and with small marshes that lack a well-defined scarp. The majority of intertidal salt marshes are in microtidal environments (Kearney and Turner 2016) and small tidal ranges increase the vulnerability of salt marshes to drowning (Kirwan et al. 2010; Ganju et al. 2017). Studies of sediment transport and deposition near bay-marsh boundaries in microtidal environments are needed.

In this paper, we combine field measurements and modeling to investigate the physical processes controlling concentrations and fluxes of suspended sediment along a tidal flat-marsh transect, as well as sediment deposition on the marsh surface, in a shallow, microtidal coastal bay (tidal range of 1.2 m). We then use the results to assess the ways in which these processes differ from those controlling deposition on

tidal creek marshes, the potential impact of increases in sea level and storminess on deposition rates for bay-fronted marshes in microtidal coastal bays, and implications for modeling sediment deposition on marshes in these systems.

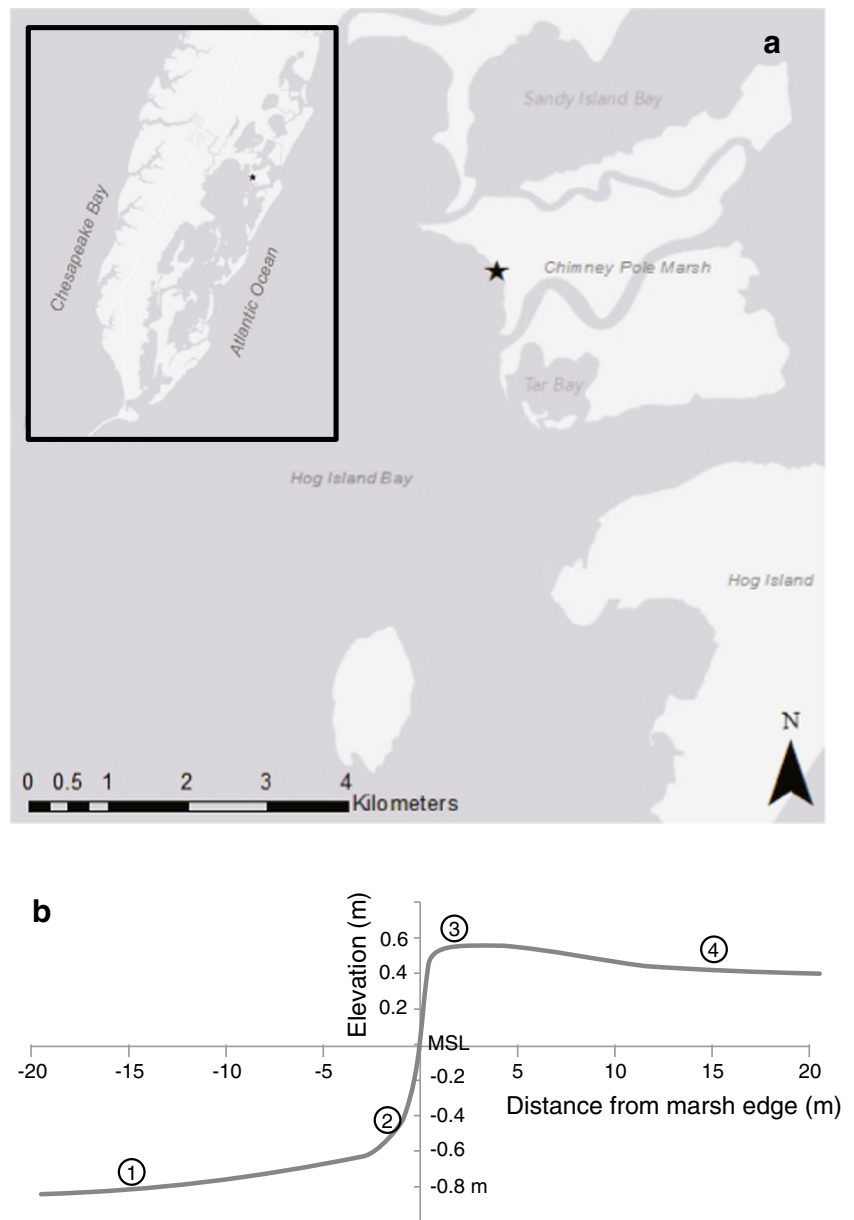
Study Site

The Virginia Coast Reserve (VCR) is a barrier-bay-marsh system that extends over 100 km along the Atlantic side of the lower Delmarva Peninsula. The VCR lacks significant fluvial sediment sources, although a recent modeling study found that fine-grained ocean sediment is imported to the bay side of tidal inlets during intense storms with large storm surge (Castagno et al. 2018). Hydrodynamic processes internally redistribute sediment among the shallow bays, barrier islands, and tidal salt marshes that comprise this system (Mariotti and Fagherazzi 2010). Wind-generated waves drive marsh-edge erosion along most of the bay-marsh boundary in the VCR (Mariotti and Fagherazzi 2013; McLoughlin et al. 2015; Priestas et al. 2010), and force episodically high suspended sediment concentrations (SSC) in the shallow portions of the bays (Lawson et al. 2007). Southerly winds are more common than northerly winds, particularly during the summertime (Fagherazzi and Wiberg 2009), but the highest wind speeds are typically associated with winter Nor'easters.

This study focuses on the bay-marsh edge along a section of Chimney Pole Marsh (CPM), a marsh island bordering Hog Island Bay (Fig. 1). The bay is fringed by salt marshes that colonize the mainland, islands, and back-barrier areas, accounting for approximately 30% of total surface area (Oertel 2001). The bay is approximately 100 km², and about 50% of the bay is less than 1 m deep at mean low tide (Oertel 2001). Tides within the bay are semidiurnal, with a mean tidal range of ~1.2 m (Oertel 2001; Lawson et al. 2007). Field measurements and modeling indicate significant spatial and temporal variations in SSC in the bay (Lawson et al. 2007; Wiberg et al. 2015). The section of the marsh edge chosen for this study is a site of several prior studies, including measurements of long-term lateral retreat of the marsh edge scarp (McLoughlin et al. 2015), marsh edge characteristics (McLoughlin 2010), and marsh surface elevation change (Wiberg 2016).

For this study, a 30-m-long transect was established that crossed an eroding marsh edge (1.5–2 m year⁻¹; McLoughlin et al. 2015) and extended from the bay to the marsh interior (Fig. 1, Table 1). Elevation along the transect slowly increases from the bay (−0.8 m above MSL) to the tidal flat (−0.5 m above MSL) across 13 m of unvegetated bay bottom, then increases rapidly across a steep scarp between the flat and the marsh platform. On the marsh, the surface elevation along the transect decreases from the marsh edge (0.55 m above MSL) to the marsh interior (0.4 m above MSL; McLoughlin 2010), which slopes downward towards a tidal creek ~200 m from the marsh edge. Given the elevation of the study site

Fig. 1 **a** Map of study site showing the location where the transect crosses the edge between Chimney Pole Marsh and Hog Island Bay (Source: *ESRI, HERE, DeLorme, MapmyIndia*). **b** Profile of marsh transect with sampling locations indicated (Table 1)



compared to mean high water (MHW \cong 0.6 m above MSL), the marsh floods primarily during spring high tides or when the mean water level is elevated due to meteorological effects.

At CPM, the marsh edge typically erodes by detachment and dislodgement by waves of the dense near-surface root mat formed by marsh vegetation. Removal of the root mat is generally followed by erosion of the weaker, underlying sediment although this underlying layer may persist for some time as a terrace-like feature with a surface elevation between that of the marsh surface and the adjacent tidal flat (McLoughlin 2010). Sediment grain size increases from the tidal flat ($D_{50} = 11.4 \pm 1.2 \mu\text{m}$) to the interior ($D_{50} = 21.6 \pm 3.4 \mu\text{m}$), as does *S. alterniflora* biomass (Table 2). Stunted vegetation along much of the bay-marsh edge differs from the typical plant

morphology on tidal creek banks, where *Spartina alterniflora* is usually taller and thicker (Leonard and Luther 1995; Christiansen et al. 2000; Morris et al. 2002).

Approach and Methods

Overview

Current, wave, water level, and turbidity measurements were made at 4 monitoring sites (1-bay, 2-tidal flat, 3-marsh edge, and 4-marsh interior) along the study transect (Table 1; Fig. 1). Measurements were recorded for 4 weeks during the summer (May–June) and early winter (November–December) seasons

Table 1 Measurements taken at each site along the transect during March 2013 (M13), November–December 2013 (N13), and March 2014 (M14)

Site Number	1			2			3			4		
Location	Bay			Tidal Flat			Marsh Edge			Marsh Interior		
Distance from Bay-Marsh Boundary	–15 m			–2 m			2 m			15 m		
Elevation relative to MSL	–0.8 m			–0.5 m			0.55 m			0.4 m		
D ₅₀ (μm)				11.4 ± 1.2			14.1 ± 2.2			21.6 ± 3.4		
Deployment:	M13	N13	M14	M13	N13	M14	M13	N13	M14	M13	N13	M14
Velocity					X	X		X	X		X	
Depth/Waves		X	X	X	X	X	X	X	X	X	X	
SSC		X	X		X	X		X	X		X	
Deposition								X	X		X	X
Biomass								X			X	
Sediment						X			X			X

of 2013, as well as in March 2014 (Table 1). Multiple instrument deployments allowed for seasonal variations in wind, hydrodynamics, and turbidity to be captured. Waves, currents, water levels, and turbidity were recorded during each deployment at some or all of the transect sites (Table 1). Wind speed and direction were measured in South Bay (Reidenbach and Timmerman 2014), about 30 km south of the study site (Fig. 1), during the entire period of the deployments. Aboveground biomass (McLoughlin 2010) and sediment deposition were measured at marsh sites 3 (edge) and 4 (interior) and a site in between. Grain size distributions were determined for sediment samples from marsh and tidal flat sites using a particle size analyzer (Beckman Coulter 2011).

Analysis and interpretation of the field data were facilitated by the use of three models. The first is a simplified model we developed to evaluate the influence of waves and vegetation on the pattern of deposition recorded on the marsh. The second is a 1-dimensional resuspension model following Lawson et al. (2007) that we used to extend our observations of suspended sediment concentrations at one depth to the full water column and to a larger range of wave, current and water depth conditions than were measured. The third is a parametric wave model for shallow-water systems (Young and Verhagen 1996a, b), which allowed us to estimate wave conditions beyond the period of our measurements, including for higher sea levels.

Measurements and Analysis of Currents, Waves and Water Levels

We used Nortek AS Aquadopp® acoustic Doppler profilers (ADPs) to measure profiles of horizontal and vertical velocities every 15 min during each deployment. A profile of velocity was recorded at specified elevations (at least every 0.1 m) beginning at 0.1 or 0.2 m above the instrument head. Multiple ADPs were deployed along the transect, providing current measurements on the tidal flat, at the marsh edge, and in the marsh interior. Vegetative interference in the measurements taken on the marsh was not a concern given the low height and density of *S. alterniflora*. No current measurements were made at the bay site (site 1; Table 1). The data were filtered by depth to ensure that the height of current measurements was less than the corrected water depth at a given time. At marsh sites 3 and 4, currents were averaged over the whole profile to obtain a mean velocity and direction. At site 2 (tidal flat), either part or all of the profile was averaged to obtain mean velocities for various depth ranges. Current-generated bed shear stresses were estimated using a drag coefficient (Lawson et al. 2007; see Appendix) and near-bed horizontal velocity components.

RBR TWR-2050 wave-tide gauges (hereafter referred to as wave gauges) were deployed above the bay, flat and marsh surfaces, sampling at either 4 or 6 Hz every 15 min for the

Table 2 Deposition measured over 4 weeks at the marsh edge and interior during the N13 and M14 deployments compared to the deposition recorded in a tidal creek marsh from June 3 to July 2, 1997

Measurement	Source	Marsh edge	Mid-marsh	Marsh interior
Deposition (g m ⁻²) over 4 weeks	N13	0 ± 0 (N = 3)	236.34 ± 145.11 (N = 3)	12.44 ± 11.61 (N = 3)
	M14	0 ± 0 (N = 3)	358.87 ± 89.67 (N = 3)	185.94 ± 104.54 (N = 3)
	Christiansen (1998)	190	N/A	80
Biomass (g m ⁻²)	N13	43.6 ± 26.8 (N = 6)	N/A	68.6 ± 25.6 (N = 6)

(Christiansen 1998). Biomass was also measured during the N13 deployment. The number of samples, N, as well as the standard deviation is reported for each measurement

duration of a given deployment. Multiple gauges simultaneously recorded waves along the transect, allowing changes in wave height from the bay to the marsh interior to be resolved. RBR software calculated depth-corrected values of significant wave height and wave period for each sampling interval. Bottom wave orbital velocities were calculated following Wiberg and Sherwood (2008). Wave-generated bed shear stresses were estimated from bottom orbital velocities using a wave friction factor (Fredsoe and Deigaard 1992; see Appendix).

Water depth was determined from pressure recorded by the ADPs and wave gauges. Pressures were corrected for atmospheric pressure (Wunsch and Stammer 1997) and referenced to mean sea level based on barometric pressure and long-term water level measurements at the nearby NOAA Wachapreague, VA tide station (tidesandcurrents.noaa.gov). The difference between predicted and observed tides recorded at the Wachapreague station provided an estimate of storm surge at the study site.

Measurements and Analysis of Turbidity, Suspended Sediment Concentration, and Flux

We used RBR dataloggers with Seapoint Sensors, Inc. auto-ranging optical backscatter sensors (OBS) to measure turbidity at sites 1 (bay) and 2 (tidal flat) along the transect. Sensors were positioned approximately 0.35 m above the bed. Campbell Scientific® OBS-3+ were used to measure turbidity over the marsh platform except at site 3 in March 2014 when an RBR sensor was used. Sensors on the marsh were positioned approximately 0.03 m above the marsh surface. For both OBS types, the data were filtered by water depth to remove measurements recorded above the water surface and during times of shallow depth when the water surface interfered with the return signal.

The OBS measured turbidity in nephelometric turbidity units (NTU). The RBR OBS (sites 1 and 2 during both deployments, and at site 3 for M14), were factory calibrated to the same NTU standards, allowing for direct intercomparison of NTU measurements at sites with similar suspended sediment properties. NTU was converted to SSC (mg L^{-1}) by independently calibrating each instrument with sediment from the site in a stirred tank with saline water over a range of sediment concentrations up to at least 300 mg L^{-1} , which were measured based on 20–25 45 mL water samples (later filtered and weighed) that were collected while turbidity was recorded (Duvall 2014; Hansen and Reidenbach 2012). Calibration regressions and related goodness-of-fit parameters are provided in Online Resource 1.

At each site, turbidity was measured at only one elevation above the bed. At the tidal flat site we used the Rouse equation (Rouse 1937) to extrapolate from the point measurements to estimated SSC profiles throughout the full

water column in order to approximate the amount of sediment in the upper water column available for deposition on the marsh (Lawson et al. 2007; see Appendix). Given the very shallow depth of flooding waters, measured turbidity on the marsh was taken as representative of the full water column. Critical shear stress was determined to be $\tau_{cr} = 0.07 \text{ Pa}$ from a plot of NTU versus total (wave and current) shear stress at site 2 (Online Resource 2).

Sediment flux between the tidal flat and adjacent marsh platform was estimated using simultaneous measurements of turbidity and velocity at site 2 for times when water surface elevation was above the level of the marsh edge. Estimated upper-water-column SSC (SSC_{UWC}) and measured current velocity at site 2 were averaged over the depth of water flooding the marsh (i.e., from the height of the marsh surface to the height of the water surface). Suspended sediment flux was calculated as the product of SSC_{UWC} and current velocity. Uncertainty in SSC and flux estimates is the result of scatter in the SSC calibration (Online Resource 1) and the use of the Rouse profile to extrapolate SSC throughout the water column at site 2 (see Appendix).

Sediment Deposition Measurements and Calculations

The amount of sediment deposited on the marsh was directly measured using tiles positioned flush with the marsh surface (e.g., Pasternack and Brush 1998) over the course of each deployment. Average deposition was calculated using 3 tiles randomly placed at sites 3 and 4, as well as a mid-marsh site in between sites 3 and 4 (~8 m from edge). Sediment on the plates was dried and weighed; mass of sediment deposited per unit area was determined as the ratio of dry weight to tile area.

Potential sediment deposition on the marsh was estimated as the product of SSC computed from turbidity measured at site 3 (marsh edge) and sediment settling velocity (see Eq. 1 below) during times when the marsh was flooded. This will tend to overestimate actual deposition because it does not account for potential entrainment over the marsh or the effect of decreasing concentration due to deposition as flooding water moves towards the marsh interior. These effects are likely to be minimized in a zone roughly 5–10 m into the marsh, allowing for attenuation of waves propagating onto the marsh platform (Möller et al. 1996, 2014) while being close enough to the edge that a roughly 0.01 m s^{-1} flow could travel the distance from the edge in a time on the order of 10 min. Estimated deposition is sensitive to the choice of settling velocity. For the deposition estimates, we used a settling velocity of 0.06 mm s^{-1} , consistent with a grain size of $10 \text{ }\mu\text{m}$ (Dietrich 1982), slightly smaller than the D_{50} at sites 2 and 3 (Table 1).

Sediment Deposition Model

We developed a simple model to explore the relative effects of vegetation and wave action on the pattern of sediment deposition observed near a bay-marsh boundary. Sediment is assumed to be well mixed in the water column over the marsh owing to velocity fluctuations associated with turbulence and wakes that form as water flows through vegetation (Nepf 1999). If we also assume that no sediment is entrained from the marsh surface (Kastler and Wiberg 1996; Christiansen et al. 2000), we can describe the change in sediment mass in the water flooding the marsh as

$$\frac{\partial M_s}{\partial t} = \frac{-w_s M_s}{h} (= -w_s C_s) \quad (1)$$

where M_s is the mass of sediment in suspension per unit area, w_s is particle settling velocity, C_s is mass concentration of sediment and h is water depth above the marsh surface. When h is constant across the transect, Eq. 1 has the solution

$$M_s = M_{s0} e^{-(w_s/h)t} \quad (2)$$

where M_{s0} is the initial mass of sediment in the water entering the marsh and t is time. Dividing both sides by h yields an expression for sediment concentration as a function of t : $C_s = C_{s0} e^{-(w_s/h)t}$ where C_{s0} is the SSC of the water flooding the marsh. Assuming the water is moving in the x direction at a given velocity u , these solutions can be transformed into mass or concentration as a function of distance, x , using the relationship $x = \int u dt$. The pattern of deposition per unit width of marsh (D) was found by differentiating $M_s(x)$:

$$D(x) = -\frac{dM_s(x)}{dx} \quad (3)$$

We assumed a simple sinusoidal tidal variation in water depth such that

$$h_0 = A \sin(\omega t_0) - E \quad (4)$$

where h_0 is the depth of water above the marsh surface at the marsh edge, $\omega = 2\pi/T_{\text{tide}}$, T_{tide} is the characteristic tidal period (12.5 h), t_0 is time relative to tidal cycle, A is a characteristic tidal amplitude, and E is marsh elevation relative to MSL. The depth and velocity of water entering the marsh varied with time, but for simplicity, we assumed that the depth and velocity would remain constant as that water crossed an unvegetated marsh platform; the effect of marsh vegetation on velocity was accounted for as described below. The velocity of water entering the marsh was defined to be out of phase with water level by $T_{\text{tide}}/4$ such that slack water conditions were reached at high tide, i.e., $u_0 = u_T \cos(\omega t)$, where u_0 is velocity at the marsh edge and u_T is the characteristic maximum tidal velocity at the marsh edge. We assumed that most

deposition would occur by high tide (Christiansen et al. 2000) and used time steps of $\Delta t_0 \cong 0.01$ hr from the time the marsh begins to flood until high tide.

To represent vegetation density on CPM, we used a Gompertz function (Gompertz 1825) of the form

$$N = N_{mx} e^{-be^{-cx}} \quad (5)$$

where N is the number of stems per area, $N_{mx} = 500$ is maximum stem density, $b = 5$ controls the location of the inflection point in the function, and $c = 0.25$ controls the rate of change of density with increasing x . Depth-averaged flow through the vegetation, \bar{u} , was defined in terms of its ratio to u_0 using the approach of Nepf (1999), which partitions bed shear stress into skin friction with the marsh surface and form drag from plant stems,

$$(1-ad)C_B \bar{u}^2 + 0.5 \bar{C}_D a d \frac{h}{d} \bar{u}^2 = ghS \quad (6)$$

where $d = 5$ mm is stem width, $a = Nd$, $C_B = 0.003$ is skin friction drag coefficient (ranges from 0.001 to 0.005 for smooth to rough surfaces), and $C_D = 1.0$ is the bulk drag coefficient for flow around cylindrical stems. Values used for stem width and density were conservative estimates (i.e., on lower end of range) based on measurements taken on CPM and other *S. alterniflora* marshes in the VCR (McLoughlin 2010; Christiansen et al. 2000). In the absence of vegetation, $C_B u_0^2 = ghS$. If we assume ghS is the same for vegetated and unvegetated flows, we can obtain a relationship for \bar{u}/u_0

$$\frac{\bar{u}}{u_0} = \left[\frac{(1-ad)C_B}{(1-ad)C_B + 0.5 \bar{C}_D a d h} \right]^{0.5} \quad (7)$$

Because stem density, reflected in values of a , varied across the marsh, \bar{u} also varied across the marsh if the marsh was vegetated.

Waves, which are attenuated over the marsh due to effects of bed friction and vegetation drag, were also considered in our deposition model. Using our wave measurements, we found that the function

$$f_{\text{attn}} = \frac{\alpha x}{1 + \alpha x} \quad (8)$$

(Möller et al. 2014) captured the fractional wave attenuation by marsh vegetation at the study site, such that $H_{sx} = (1 - f_{\text{attn}})H_{s0}$, where H_{sx} is significant wave height a distance x from the marsh edge, H_{s0} is significant wave height measured on the tidal flat adjacent to the marsh and the constant $\alpha = 1/3$.

We calculated the pattern of deposition in the presence and absence of both waves and vegetation. For these calculations we set $w_s = 0.06$ mm s⁻¹, $u_T = 0.05$ m s⁻¹, $C_{s0} = 0.06$ g L⁻¹, $A = 0.7$ m, $E = 0.5$ m above MSL, $T_{\text{wave}} = 2$ s, and assumed that when $h < H_{s0}$, $H_{s0} = h$. These assumptions are reasonable

based on sediment analysis, topography, and current, wave, turbidity and water-level measurements made at our study site.

To calculate deposition for each tidal time step Δt_0 , we (1) determined $M_s(t)$ using Eq. 2, with h given by Eq. 4; (2) converted time since initiation of flooding (t) to distance across the marsh (x) stepwise, based on \bar{u} calculated using Eq. 7 for stem density $a(x)$; (3) converted $M_s(t)$ to $M_s(x)$; and (4) calculated the pattern of deposition using Eq. 3. To get total mass per unit marsh width, deposition was multiplied by the flux of water during each tidal time step, $u_0\Delta t_0$. The process was continued for each tidal time step, with h varying as indicated in Eq. 4 from mid-tide to high tide. After deposition was calculated for each tidal time step, total deposition was determined by summing over all time steps for that part of the tidal cycle at each location along the flow path.

Extension of Observations to Longer Time Scales and Other Forcing Conditions

We used the Young and Verhagen (1996a, b) parametric model for finite depth, fetch-limited wave growth to characterize wave conditions at the study site for water depths and wind conditions beyond those sampled in our field observations. This model has been tested and used in several previous studies in the VCR (Fagherazzi and Wiberg 2009; McLoughlin et al. 2015; Kirwan et al. 2016; Leonardi et al. 2016). The model was run using 3 wind speeds (5, 10, 15 m s⁻¹) and for depths ranging from 0 to 3 m above the tidal flat. A fetch of 10 km was used, consistent with westerly winds (i.e., the direction associated with the largest wind-waves) at the study site (Fig. 1).

Wave heights and periods obtained from the parametric model (Young and Verhagen 1996a, b) were used to estimate wave-induced bed shear stress following the method of Wiberg and Sherwood (2008). For each wind speed and water depth combination, a full wave spectrum was estimated based on significant wave height and peak period and the Donelan wave spectrum (Donelan et al. 1985; Wiberg and Sherwood 2008). Wave-generated bottom orbital velocity was calculated from the sum of the contribution of each frequency band of the surface wave spectrum following Wiberg and Sherwood (2008). Wave-generated bed shear stress was then calculated from bottom orbital velocity as described in the Appendix.

To estimate potential deposition under the given range of wind and depth values, average values of current shear stress ($= 9.4 \times 10^{-4}$ Pa) and current shear velocity ($= 8.1 \times 10^{-4}$ m s⁻¹) were calculated for the tidal flat during the period of observation. These values, along with wave shear stresses calculated as described above, were used in the Rouse equation to estimate SSC profiles (see Appendix). Total sediment mass in the upper water column was approximated by integrating the Rouse profile for the portion of the water column

above the height of the marsh. This provided an estimation of mass available for potential deposition on the marsh surface.

Results

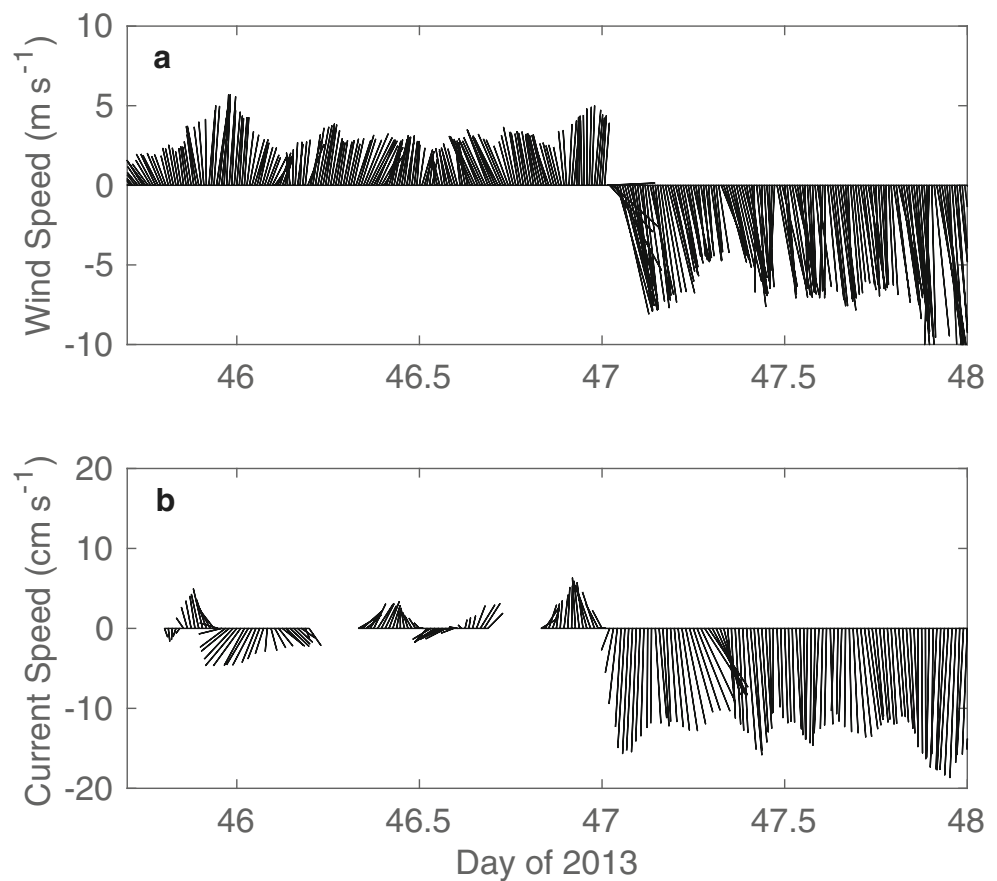
Currents and Water Levels

There was a strong effect of wind speed and direction on tidal flow at the study site. Moderate southerly winds during March 2013 (deployment M13) corresponded with periods of alternating northward flood and southward ebb tidal currents at a tidal flat site ~ 0.4 km south of the transect (Fig. 2). Conversely, in the presence of stronger northerly winds, currents flowed towards the south, regardless of tidal phase, though with tidally varying speeds. Average current speeds during times of weaker southerly winds were less than half (< 5 cm s⁻¹) the speeds during periods of stronger northerly winds (> 10 cm s⁻¹), and current speed increased during spring tide. In addition to wind speed and direction, marsh edge morphology also influenced current direction, as tidal flow at site 2 moved primarily in the NE-SW direction (Fig. 3a), i.e., the primary orientation of the marsh edge, when water surface elevations were below the height of the marsh platform. When the marsh was flooded, variability in current direction at site 2 increased in the portion of the water column above the height of the marsh platform (Fig. 3b).

During neap tide, the marsh rarely flooded unless there was a storm surge event. During the November–December 2013 (N13) (March 2014 (M14)) deployment, the marsh was flooded (water-surface elevation > 0.55 m MSL) approximately 17% (19%) of the total time, and of the 27 (24) tidal cycles when the maximum water depth over the marsh edge was > 0.05 m, almost all occurred either during spring tide (N13, 20 cycles; M14, 16 cycles) or during neap tide if the measured water level exceeded the predicted tide (N13, 6 cycles; M14, 6 cycles).

On the marsh platform, current direction was highly variable during flood and ebb tide at our monitoring site closest to the bay-marsh boundary (site 3). In addition to variable wind speed and direction, this was likely influenced by the irregular edge morphology, such as the relatively large embayment immediately north of the transect. Current magnitude and direction were E-SE at less than 2 cm s⁻¹ during both flood and ebb tide at our interior marsh site (site 4), indicating that the marsh interior floods from Hog Island Bay and ebbs into the tidal creek ~ 200 m behind the transect. Faster draining of the creek compared to the marsh, as well as the relatively steep downward slope of the marsh surface behind transect, likely forced currents in the direction of the tidal creek. This pattern agreed with our ADP measurements taken at a marsh site ~ 0.4 km south of the transect.

Fig. 2 **a** Wind speed (m s^{-1}) recorded in South Bay and plotted as the direction towards which the wind is blowing. **b** Current speed (cm s^{-1}) plotted as the direction towards which the water is flowing. Currents were averaged over the entire height of the water column and recorded south of the transect during the M13 deployment



Waves and Bed Shear Stress

Westerly winds (180° – 360°) blowing across Hog Island Bay produced the largest waves at the study site (median $H_s = 0.26$ m; mean $H_s = 0.26$ m; Fig. 4), because that is the direction with the greatest fetch given the orientation of the marsh edge at CPM (Fig. 1). There are barrier islands (e.g., Hog Island) and marshes upwind of the marsh edge at CPM for easterly and northerly winds, thus inhibiting wave formation due to limited fetch (McLoughlin et al. 2015). High wind speeds (≥ 8 m s^{-1}) occurred during 12% of the N13 deployment (34% of the M14 deployment) and produced larger waves than lower wind speeds (Fig. 4). A wind threshold for significant wave-generated resuspension of about 8 m s^{-1} was previously determined by Lawson et al. (2007) for a site in Hog Island Bay. Mean wave heights for each interval of wind direction were up to 4 times higher under high wind speed conditions compared to low wind speed conditions (Fig. 4).

Bed shear stress on the tidal flat was sensitive to wind speed and direction. Maximum bed shear stress occurred when winds blew from a W-NW direction at speeds exceeding 8 m s^{-1} and when water surface elevations were around MHHW (0.68 m above MSL at Wachapreague, VA; Fig. 5). For higher water surface elevations, bed shear stress declined with increasing surface elevation (Fig. 5). When wind speeds

were less than 8 m s^{-1} , total bottom shear stress was lower and did not differ significantly with water surface elevation due to low wave activity.

Wave transformation along the transect from site 1 to site 4 was recorded in November–December 2013 (Fig. 6). As waves propagated across the tidal flat (site 1 to 2), wave height increased by an average of 33% due to wave shoaling. After the waves crossed the marsh edge, their height rapidly diminished owing to attenuation by marsh vegetation. Wave heights recorded at site 1 were reduced by an average of 67% and 83% at sites 3 and 4, respectively (Fig. 6b).

During N13 (M14), wave shear stress exceeded the threshold for sediment resuspension (0.07 Pa) at site 2 27% (16%) of the total time (Fig. 7). For 8% (16%) of these times, wave shear stress also exceeded 0.07 Pa at site 3, indicating that the depth was great enough to sustain wave energy across the bay-marsh boundary. While wave heights on average were greater at site 2 than at site 3 during times when the marsh was flooded (Fig. 6), bed shear stresses generated by those waves were generally greater at site 3 than at site 2 owing to the shallower depths at site 3. Wave shear stress at site 3 exceeded 0.07 Pa 5% of the total time during the N13 deployment (41% of inundation time) and 12% of the total time (100% of inundation time) during the M14 deployment. Bed shear stresses estimated from surface waves near the marsh edge are likely to

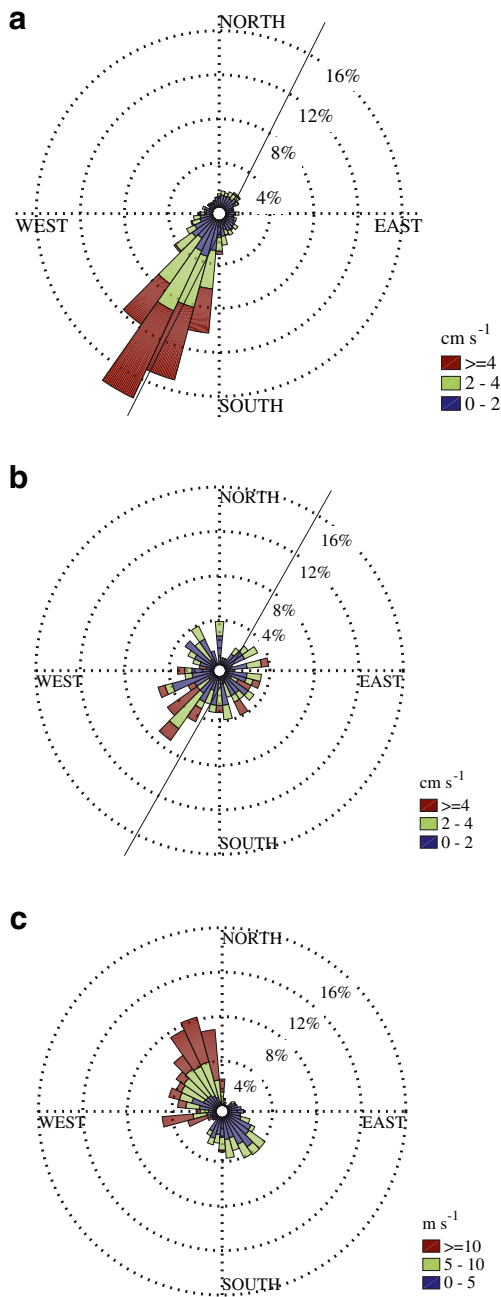


Fig. 3 Current direction (deg) and speed (cm s^{-1}) measured at site 2 during the M14 deployment for (a) the lower water column (i.e., below the marsh surface height; and (b) the upper water column (i.e., above the marsh surface height; middle). Diagonal line indicates marsh edge orientation and position relative to site 2. c Wind direction (deg) and speed (m s^{-1}) recorded in South Bay during the M14 deployment

be reasonable given low vegetation densities and heights at site 3. Therefore, based on shear stress alone, sediment remobilization at the marsh edge is possible. At site 4, bed shear stresses estimated from surface waves exceeded 0.07 Pa 1% of the time in N13 (10% of inundation time; no M14 measurements); however, these stresses may be overestimated given the presence of denser, taller vegetation at site 4.

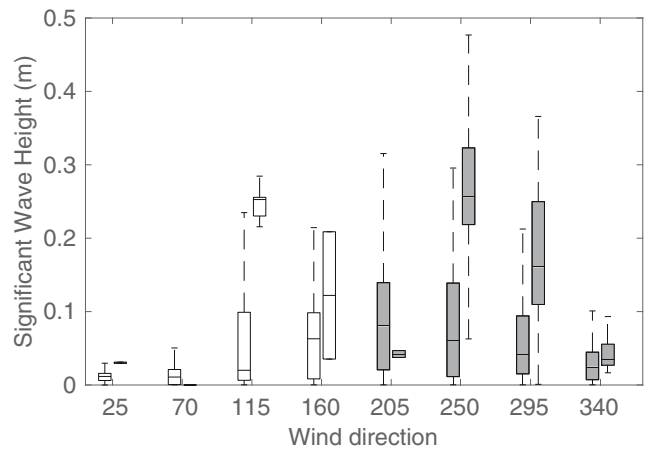


Fig. 4 Significant wave height (m) separated into 8 wind direction (deg) intervals of 45 degrees each. Within each wind direction interval, significant wave heights measured during times of low (left, $< 8 \text{ m s}^{-1}$) and high (right, $> 8 \text{ m s}^{-1}$) wind speeds are shown. Shading indicates westerly winds blowing across Hog Island Bay. Data were recorded at site 2 during the N13 deployment

Turbidity, Suspended Sediment, Flux, and Deposition

Measured turbidity increased episodically in response to elevated bottom shear stress during wave events; tidal currents had little effect on turbidity (Fig. 7). At sites 1 (bay) and 2 (flat), measured turbidity reached values > 10 times higher than deployment averages when relatively large wave events occurred during neap tide cycles (Fig. 7). Similar wind conditions during spring tide or storm surge events resulted in smaller bottom shear stresses at both sites. High wind conditions produced turbidity values at site 1 that were 10–15% lower than values at site 2. There was a positive correlation

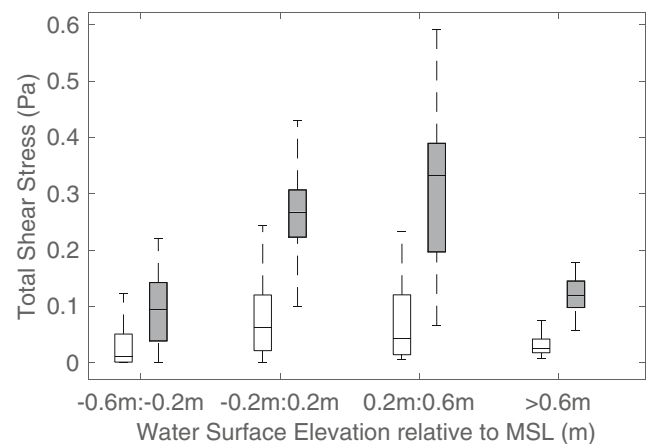
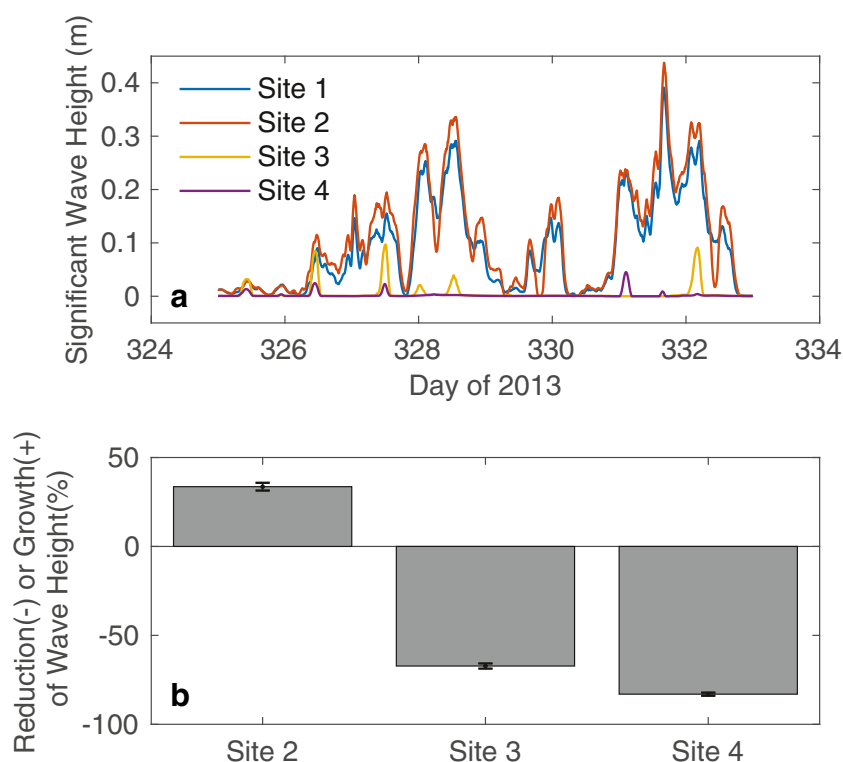


Fig. 5 Total bottom shear stress (Pa) as a function of water surface elevation relative to MSL during times when the wind blew across Hog Island Bay from a W-NW direction (240–305 degrees). For each water surface elevation interval, data are separated into low ($< 8 \text{ m s}^{-1}$, white boxes) and high ($> 8 \text{ m s}^{-1}$, shaded boxes) wind speed groups. Data were recorded at site 2 during the N13 deployment

Fig. 6 **a** Significant wave height (m) during two large wave events, which occurred during the N13 deployment. **b** Average growth or reduction in significant wave height during N13 given as a percentage of the initial height recorded at site 1. Error bars show the 95% confidence interval ($1.96 \times \text{standard error}$)



between turbidity and wave-induced shear stress at sites 1 and 2 during N13 and M14 (e.g., Fig. 8). The relationship between turbidity and bottom shear stress was complicated by the fact that measured turbidity remained elevated after bed shear stress declined due to low settling velocities and changing tidal stage. To reduce the effect of tidal stage on turbidity, we focused our comparison of bed shear stress and turbidity on a mid-range of depths (0.4–0.8 m for site 2; Fig. 8).

Turbidity and suspended sediment concentration (SSC) are significantly correlated for all OBS sensors and sites (Online Resource 1). Peak NTU during both deployments was close to 300 at site 2, corresponding to $\text{SSC} = 330 \pm 100 \text{ mg L}^{-1}$ (95% confidence limit on predicted SSC based on calibration data for sensor R75; Online Resource 1). The large uncertainty is due to scatter in the calibration. Differences between measured turbidity at sites 1 and 2 are independent of the calibration and, owing to the similarity in the calibration regressions for the OBSs at these sites, likely also correctly reflect relative differences in SSC between these sites.

The largest resuspension events on the tidal flat did not elevate turbidity on the marsh because the events occurred during neap tide when the marsh rarely flooded. Turbidity at the marsh edge (site 3) was well correlated ($r^2 = 0.84$) with turbidity over the flat (site 2) for periods of marsh inundation during both deployments when wind speeds were high enough to force wave-driven resuspension ($\geq 8 \text{ m s}^{-1}$; filled symbols, Fig. 9a, b). Turbidity at sites 2 and 3 also fell within these bounds for a large fraction of tides when the marsh was

inundated and wind speeds were lower ($< 8 \text{ m s}^{-1}$; open circles). A comparable level of agreement is evident when comparing upper-water-column estimates of SSC (SSC_{UWC}) at site 2 with estimated SSC at site 3 based on Rouse profile estimates using calibrated SSC, and scaling the confidence interval for NTU at the two sites ($\pm 7 \text{ NTU}$) by the slope of the calibration regressions (2.6 ± 0.4) for $\text{NTU} < \sim 50$ for both sites (Online Resource 1) (Fig. 9c, d). The low wind speed cases indicated with red symbols in Fig. 9c, d occurred during tides when waves were too small to produce significant resuspension on the flat (site 2) but were large enough in the shallower water over the marsh edge (site 3) to resuspend sediment either from the marsh-edge scarp or the marsh surface.

Suspended sediment flux in the upper water column over the tidal flat (water surface elevations above that of the marsh surface) was more variable during M14 than N13 (Fig. 10a, b). The winds during spring tide conditions in N13 were generally low or from the north (Fig. 7a), resulting in relatively small suspended sediment fluxes with net transport in the marshward and southward directions (Fig. 10c). The stronger winds that characterized the M14 deployment (Fig. 7e) resulted in larger but variably directed fluxes (Fig. 10b) and net transport in a direction along the marsh edge (Fig. 10c). While specific values of flux are subject to uncertainty in calibrated values of SSC, trajectory pathways are not. Overall the flux of sediment near the marsh edge appears generally advective in N13, carrying sediment from the upper

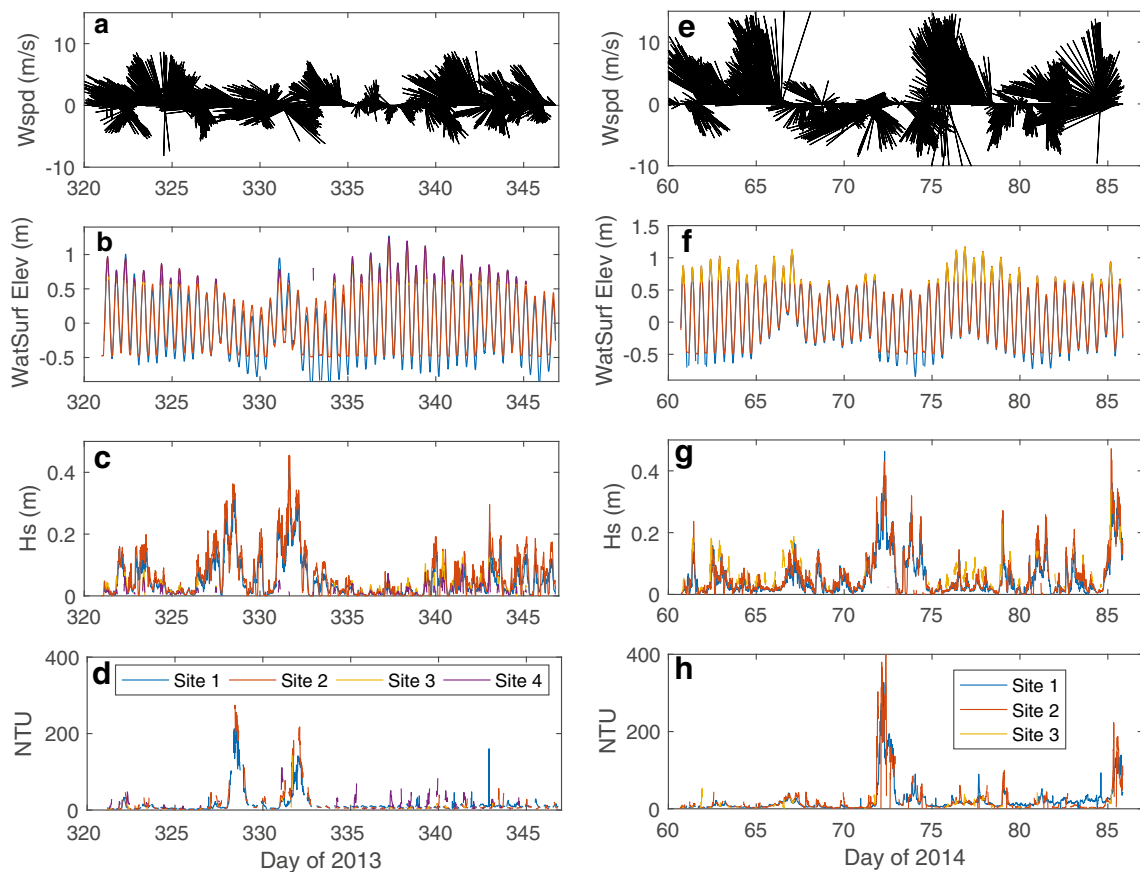


Fig. 7 a, e Wind vectors; b, f water surface elevation above the tidal flat (m); c, g significant wave height (m) and d, h turbidity (NTU, 0.35 m above the bed) recorded during deployment N13 (a–d) and M14 (e–h). Breaks in the turbidity record indicate times when the instrument was out of the water

water column over the flat onto the marsh, whereas the flux appears generally diffusive in M14, with winds driving a more random pattern of transport. In either case, turbidity over the marsh near the edge was similar to turbidity in the upper water column over the flat during most of the time when the marsh was flooded (Fig. 9a, b).

Sediment transported onto the marsh did not accumulate near the marsh edge, as recorded by sediment deposition plates installed during the N13 and M14 deployments (Table 2). This agrees with long-term surface elevation table (SET; Lynch et al. 2015) data collected approximately 0.4 km south of the transect (Wiberg 2016) and is consistent with our observation that bed shear stress near the marsh edge (\sim less than 3 m from the edge) may at times be high enough to mobilize sediment or at least prevent deposition. Maximum deposition occurred at the mid-marsh sediment plates (\sim 8 m from the edge), with additional deposition further into the marsh interior (\sim 15 m from the edge). This observed pattern of deposition differs from a tidal creek marsh where deposition is typically maximized at the creek bank levee (Table 2; Fagherazzi et al. 2013).

Sediment deposition on the marsh was estimated from the product of SSC at site 3 and estimated settling velocity

(0.06 mm s^{-1} ; see “Sediment Deposition Measurements and Calculations”) for N13 and M14 (Fig. 9e, f, solid lines); deposition was similarly calculated using estimated upper-water-column SSC (SSC_{UWC}) at site 2 (Fig. 9e, f, dashed lines). [The amount of estimated deposition in each 15-min interval

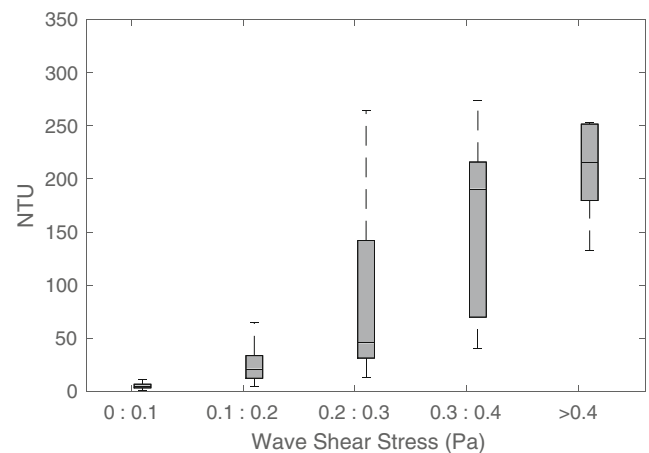


Fig. 8 Turbidity as a function of wave shear stress (Pa) recorded at site 2 during the N13 deployment for a mid-range of water depths spanning mean sea level (0.4–0.8 m)

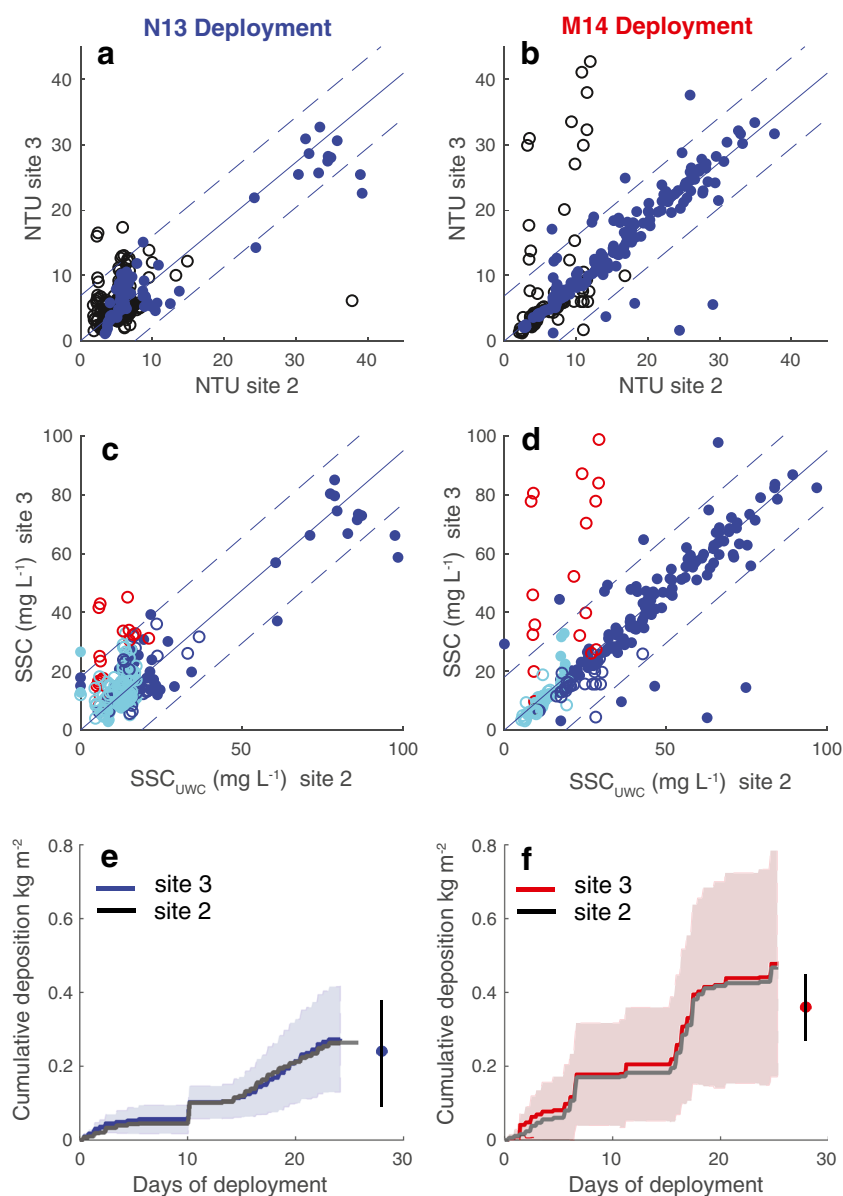


Fig. 9 Comparison of turbidity at sites 2 and 3 during **a** N13 and **b** M14 for times when the marsh was flooded and wind speed $\geq 8 \text{ m s}^{-1}$ (filled symbols); dashed lines indicate 95% confidence interval on predicted NTU-site 3 given NTU-site 2 for these conditions. Open symbols indicate conditions when the marsh was flooded and wind speed $< 8 \text{ m s}^{-1}$. Comparison of estimated SSC in the upper water column (SSC_{UWC}) over the flat (site 2) vs. estimated SSC over the marsh near the edge (site 3) during **c** N13 and **d** M14 for higher (filled symbols) and lower winds (open symbols) as in 9a, b. Dashed lines are scaled from those shown in 9a, b by the common slope (2.6) of the calibration relationships for $\text{NTU} < \text{NTU}_{\text{BP}}$ (Online Resource 1). Light blue open symbols in 9c, d indicate

flooding tides accompanied by low waves and low turbidity while flooding tides characterized by shallow inundation depths and peak SSC at the marsh edge that is more than twice the peak SSC_{UWC} when $\text{SSC}_{\text{UWC}} < 20 \text{ g L}^{-1}$ are indicated by red open symbols. Estimated deposition during **e** N13 and **f** M14 based on SSC at the marsh edge (site 3, colored lines) and SSC_{UWC} over the flat (gray lines). The shading indicates the range of the estimates based on root-mean-square error (RMSE). The symbols on the right side of 9e, f are mean values of measured deposition at the mid-marsh site (Table 2) with vertical lines indicating standard deviation

of the record never exceeded the mass of sediment per unit area in the water at site 3 at that time, estimated as SSC times water depth.] The shaded band around the estimates reflects the root-mean-square error (RMSE) associated with the NTU-SSC calibrations (Online Resource 1). For comparison, mean and standard deviation of measured deposition at the mid-marsh site (Table 2) are also indicated in Fig. 9e, f. Deposition estimates

based on SSC at site 3 and on SSC_{UWC} at site 2 are almost the same. Estimated deposition overlaps measured values, but the large range of estimated values due to the relatively large RMSE for M14 makes it difficult to draw a conclusion about level of agreement. While specific values of estimated deposition are sensitive to uncertainty in SSC calibrations and the choice of settling rate, the ratio of estimated deposition in

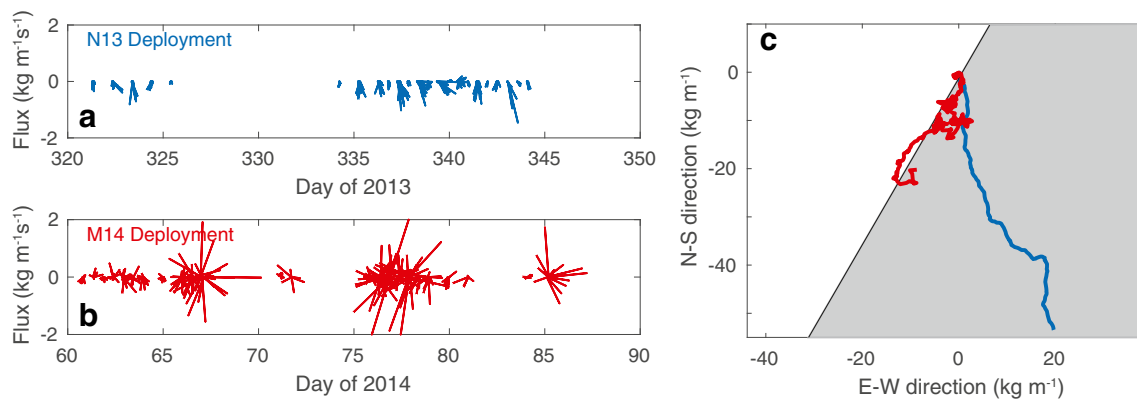


Fig. 10 Suspended sediment fluxes in the upper water column (above the elevation of the marsh surface) over the tidal flat (site 2) during **a** N13 and **b** M14; an upward pointing vector indicates northward transport. **c**

Progressive flux trajectories (cumulative integrated flux) during N13 and M14. Shading indicates the location of the marsh (as opposed to bay) relative to the trajectories

N13 to M14, which can be calculated directly from measured turbidity, is not. The ratio based on measured turbidity (0.57) is similar to the ratio of measured deposition at the mid-marsh site (0.66), indicating that measurements of turbidity over the tidal flat and marsh and measurements of deposition over the course of each deployment are generally consistent.

Sediment Deposition Model

Deposition patterns predicted by our marsh sediment deposition model depend on marsh surface elevation and particle settling velocity as well as the presence or absence of vegetation and waves. Our calculations assume a vegetation distribution typical of many bay-fronted marshes in the VCR, with short, low-density *S. alterniflora* near the marsh edge that increases in density and stem height away from the edge until a relatively constant height and density are reached (Fig. 11). With vegetation and no waves (marsh elevation = 0.5 m above MSL; settling velocity = 0.06 mm s^{-1} , consistent with deposition estimates above), deposition begins at the marsh edge, with a modestly higher value several meters inland. Higher values of settling velocity shift the depositional maximum to the edge. This pattern of deposition is similar to that found on many tidal creek marshes (Christiansen et al. 2000; Leonard 1997; Friedrichs and Perry 2001; Fagherazzi et al. 2013).

Adding the effect of surface waves into the depositional model eliminates nearly all deposition within several meters of the marsh edge, displacing the point of maximum deposition inland (about 6 m for the parameter values used in the example shown in Fig. 11), even for relatively small waves ($H_{s0} = 0.1 \text{ m}$), which is consistent with the pattern of deposition recorded by the sediment plates (Table 2). This occurs because wave-generated bed shear stresses near the marsh edge exceed the critical shear stress (0.07 Pa), creating a zone of non-deposition or possibly even erosion. When both waves and vegetation are present, deposition within the marsh

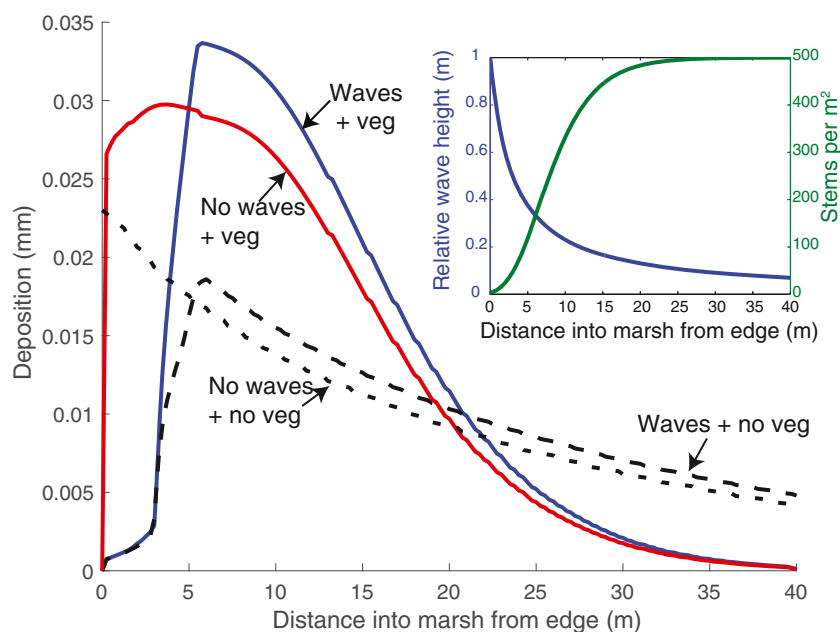
interior is enhanced due to the added effect of vegetation slowing flow velocities and trapping sediment. In the absence of vegetation, maximum deposition is still shifted about the same distance inland from the edge, but more sediment is carried further into the marsh interior (Fig. 11).

Dependence of Bed Shear Stress and SSC on Water Surface Elevation

To explore the influence of water surface elevation on sediment transport for conditions beyond those directly measured (e.g., influence of storms or RSLR), wave shear stress was estimated for a range of water depths using the parametric wave model (Young and Verhagen 1996a, b), a 10 km fetch (consistent with the fetch for winds from the west and north-west) and 3 wind speeds (5 m s^{-1} , 10 m s^{-1} , and 15 m s^{-1}) (Fig. 12a). The maximum water depth at which orbital motions due to surface wind waves are present is determined by wavelength, which depends on wind conditions and water depth. Wave shear stress at a given depth is positively correlated with wind speed, while for a given wind speed, there is a depth where wave shear stress is maximized, with lower shear stresses at greater depths. As wind speed increases, the depth at which wave shear stress is maximized also increases. Maximum wave shear stress occurs at depths of 0.6 m ($\tau_{\text{wave}} = 0.11 \text{ Pa}$), 1.2 m ($\tau_{\text{wave}} = 0.56 \text{ Pa}$), and 1.6 m ($\tau_{\text{wave}} = 1.02 \text{ Pa}$) for the low, medium, and high wind speed scenarios, respectively.

Given the relationship between depth and wave shear stress, changes in water column sediment mass (Fig. 12b) were estimated for a variety of water surface elevations greater than the marsh height. No results are shown for water surface elevations below the elevation of the marsh platform (water depths < 1 m assuming a mean elevation of 0.5 m below MSL for the tidal flat and an elevation of 0.5 above MSL for the marsh platform). Despite lower shear stress and SSC at water

Fig. 11 Modeled distribution of sediment deposition on the marsh in the presence and absence of both waves and vegetation, and the variation in relative wave height and vegetation with distance into the marsh used in the model calculations (inset). Values for model parameters are provided in Methods



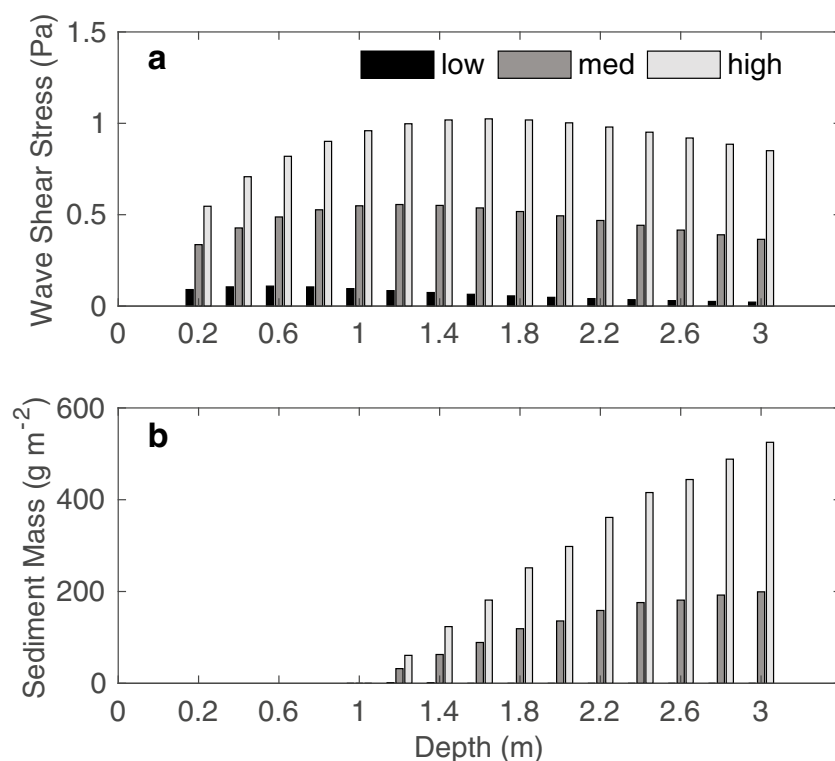
depths greater than the depth associated with the maximum wave shear stress, sediment mass in the upper water column increases with increasing water depth for the medium and high wind cases. This pattern arises because an increase in the depth of water flooding the marsh more than offsets the slightly lower SSC in that water. No sediment is in suspension for the low wind cases because the bed shear stress is below the threshold of motion.

Discussion

Controls on Turbidity and SSC in Water Flooding Bay-Fronted Marshes

Tidal flat turbidity is highly correlated with wave shear stress and minimally correlated with current shear stress, the latter being the primary control of SSC in tidal

Fig. 12 a Wave shear stress given for a range of water depths above the tidal flat and 3 wind speeds. **b** Sediment mass (g m^{-2}) as a function of water depth above the tidal flat for water flooding the marsh (elevation > 1 m), assuming the marsh remains at its current elevation



creeks (Christiansen et al. 2000). The results from this study indicate a strong correlation between wind direction and wave height, whereby the largest waves form when winds blow across Hog Island Bay from a direction with a long fetch (i.e., westerly winds at our study site) at relatively high speeds ($\geq 8 \text{ m s}^{-1}$). The largest waves we recorded did not coincide with storm surge conditions, likely due to the fact that storm surge in the Virginia coastal bays generally occurs when winds blow from the northeast (Fagherazzi and Wiberg 2009; Fagherazzi et al. 2010), a direction associated with very short fetch at the study site.

While waves control turbidity on the tidal flat, tides control inundation of the marsh. The wind events that generated the highest bed shear stresses on the tidal flat had little impact on marsh deposition at our site because these events typically occurred during neap tides when the marsh barely flooded. For example, the storm event that occurred during the N13 deployment (Fig. 6a), with significant wave heights greater than 0.3 m, resulted in peak SSC of $300 \pm 100 \text{ mg L}^{-1}$ over the tidal flat (Fig. 7d). Nevertheless, very little sediment reached the marsh surface during that event due to infrequent flooding. Similar wave events during spring tide or storm surge resulted in lower turbidity and SSC due to lower wave-induced bottom stresses. Therefore, our data indicate a nonsynchronous relationship at our study site between the highest wave-driven turbidity on the tidal flat, which increases sediment availability, and prolonged marsh inundation, which increases sediment delivery. At times when the water level was lower than the elevation of the marsh surface, current direction was along the marsh edge. Thus, the marsh edge scarp may play an important role in redirecting sediment resuspended from the tidal flat along the marsh edge to be deposited in another location further away.

During times when the marsh did flood—primarily during spring high tides—and wind speeds were relatively high ($\geq 8 \text{ m s}^{-1}$), turbidity measured over the flat (site 2) and over the marsh edge (site 3) were well correlated (filled symbols, Fig. 9a, b). This is also reflected in the relationship between estimated SSC in the upper water column over the tidal flat (SSC_{UWC}) and in the water overlying the marsh near the edge (filled symbols, Fig. 9c, d). During these conditions, measured turbidity reached about 40 NTU. While considerably lower than peak turbidity on the tidal flat during resuspension events when the marsh was not flooded (Fig. 7), these moderately high turbidity flooding tides were responsible for the majority of sediment imported from the bay to the marsh.

Most lower wind conditions ($< 8 \text{ m s}^{-1}$; open symbols) were associated with low waves and low turbidity and SSC at both sites (80% of flooding tides in N13; 46% in M14) (Fig. 9c, d; light blue symbols). Values of peak SSC_{UWC} in the range $15\text{--}20 \text{ mg L}^{-1}$ were typical at site 2 for flooding tides during low wind conditions. About 10% of flooding tides with lower wind speeds were characterized by peak turbidity at site 3 that

was more than twice that measured at site 2. These are tides, mostly of short duration and shallow marsh inundation depths, that occur when winds are too low to generate waves able to resuspend sediment from the tidal flat but large enough to generate waves able to mobilize sediment from the marsh-edge scarp or marsh-edge platform (red open symbols in Fig. 9c, d). These locally high SSC conditions at the marsh edge may be associated with erosion and redistribution of sediment comprising the marsh-edge scarp and/or sediment deposited on the marsh edge platform. Whether or not remobilization occurs on the marsh edge depends on a range of factors that can influence sediment mobility on intertidal surfaces including wave pumping, consolidation, and biotic effects related to plants and invertebrates living on the marsh (Pestrong 1969; Paramor and Hughes 2004; Wilson et al. 2012; Wiberg et al. 2013).

The good agreement between estimated SSC_{UWC} over the tidal flat and in the water overlying the marsh near the edge (Fig. 9c, d) during flooding tides with relatively high winds suggests that sediment suspended in the upper water column over the tidal flat, which was primarily controlled by wind and wave conditions in the bay, was transported onto the marsh as it became inundated. During N13, suspended sediment fluxes over the tidal flat were generally marshward and similar in magnitude and direction for most flooding tides (Fig. 10a). Average fluxes during N13 were smaller than during M14, but owing to their dominantly marshward orientation, produced a larger cumulative marshward flux than was found during M14 (Fig. 10c). Upper-water-column fluxes were greatest during episodically high northerly winds, which were accompanied by storm surge during spring tides in M14. Variability in the direction of upper-water-column currents during this deployment resulted in variably directed fluxes (Fig. 10b) with an overall along-edge trend (Fig. 10c). Despite the differences in the character of the fluxes during the two deployments, the similarity in the relationship between SSC_{UWC} over the tidal flat and SSC in the water overlying the marsh edge for N13 and M14 (Fig. 9c, d) indicate similarly effective transport of suspended sediment from the flat to the marsh surface during flooding tide conditions.

Deposition on Bay-Fronted Marshes

Marsh deposition is maximized in the presence of both high SSC and high water levels, which together control the mass of sediment available for deposition and the length of time over which deposition can take place (e.g., Christiansen et al. 2000; Pratolongo et al. 2010; Fagherazzi et al. 2013; Schuerch et al. 2013; Butzeck et al. 2015). The higher measured deposition at our site during M14 compared to N13 is primarily the result of higher SSC at the marsh edge during M14. A simple estimate of deposition based on the product of SSC at the marsh edge (calculated from measured turbidity) and particle settling rate

(estimated as roughly 0.06 mm s^{-1} based on a representative grain size of $10 \text{ }\mu\text{m}$) yielded cumulative deposition estimates with a range (based on root-mean-square error (RMSE)) that overlapped deposition measured 8 m inland from the marsh edge (mean \pm standard deviation), though large RMSE for the M14 estimates complicates that comparison (Fig. 9f). The ratio of estimated N13 and M14 deposition (0.66), which can be made directly from measured turbidity, thereby avoiding uncertainties associated with values of SSC and settling velocity, is in general agreement with the ratio of mean measured deposition at the mid-marsh site (0.57) (Fig. 9e, f).

The time series of cumulative deposition is marked by intervals of more rapid deposition associated with flooding tides (spring tides or neap tides and storm surge) and higher winds, and intervening periods of little to no deposition during neap tides or lower winds. It is worth noting that spring tide high water levels during both deployments were often higher than predicted owing to meteorological effects.

The observed pattern of deposition at our site differs from the pattern commonly observed at tidal creek marshes (e.g., Leonard 1997; Christiansen et al. 2000; French and Spencer 1993; Fagherazzi et al. 2013; Butzeck et al. 2015), with no net deposition recorded at our marsh edge site (3 m from the marsh-edge scarp), maximum deposition at a site 8 m marshward from the edge, and lower deposition at our most interior site (15 m from the marsh edge) (Table 2). The results from our marsh deposition model (Fig. 11) indicate that this pattern is largely due to the effects of waves that propagate across the marsh edge. The model we used to estimate depositional patterns on bay-fronted marshes differs from one appropriate for marshes bordering tidal channels (e.g., Fagherazzi et al. 2013) only in the specified distribution of vegetation with distance from the marsh edge (observed marsh vegetation sparser and shorter near the edge than in the interior) and the presence of waves. The addition of waves moves the depositional maximum inland, largely because near-edge shear stresses on the marsh become sufficiently large to prevent deposition or even entrain sediment from the marsh surface. Further support for net erosion near the marsh edge is found in longer-term surface elevation measurements collected near the marsh edge just south of the study area, where the marsh-edge surface is lowering over time (Wiberg 2016).

The width of the zone of non-deposition near the marsh edge in our model is largely a function of wave-generated shear stresses on the marsh surface, which depend on wave height and water depth. Small waves and deeper water contribute to lower shear stresses that allow deposition near the marsh edge whereas larger waves and shallower water yield higher shear stresses and a broader zone of non-deposition or erosion, potentially rendering the marshes more susceptible to future drowning as sea level rises. The distribution of deposition within the marsh depends on particle settling velocity and

vegetation density. Faster settling velocities and greater vegetation densities produce thicker, narrower deposits.

Uncertainty in Suspended Sediment Concentrations

Our estimates of SSC over the tidal flat and marsh, and associated fluxes, are subject to uncertainty associated with the calibration of the turbidity sensors, which we used to relate NTU to SSC. Regression parameters, coefficients of determination (r^2), and root-mean-square errors (RMSE) for each turbidity sensor are provided in Online Resource 1. SSC was significantly correlated with NTU for each sensor ($r^2 = 0.75\text{--}0.93$, $p < .05$, for linear fits to all calibration points; $r^2 = 0.85\text{--}0.96$, $p < .05$, for bi-linear fits to calibration data that were significantly segmented; see Online Resource 1). RMSE was relatively high ($\geq 20 \text{ mg L}^{-1}$) for linear or bilinear fits to calibrations over the full range of 0–300 NTU owing to scatter in the calibrations. For this reason, we have emphasized temporal and spatial trends in measured turbidity, rather than calibrated SSC, where possible, as our sensors at sites 1 and 2, and at site 3 in M14, were factory calibrated to common NTU standards. Regression parameters for calibrations of these sensors are not significantly different, reflecting the similar response of these OBSs and the similar sediment at sites 1, 2, and 3 (Table 2). Regression slopes are also the same (2.6 ± 0.4) when NTU is roughly < 50 (below breakpoint in segmented regression) for OBSs used at sites 1, 2, and 3 during N13 and M14. This supports our ability to directly compare measured turbidity at sites 2 and 3 (N13 and M14) during conditions when the marsh was flooded even if there is a greater level of uncertainty as to the specific values of SSC at those times.

Additional uncertainty in estimated upper-water-column SSC over the tidal flat comes from the use of the Rouse equation to extrapolate from the elevation of the turbidity sensor (0.35 m above the bottom) to the portion of the water column above the elevation of the marsh. Of the 3 grain size fractions used in the Rouse profile calculation (7, 25, and $100 \text{ }\mu\text{m}$; see Appendix) only the finest fraction has a sufficiently low settling velocity (0.03 mm s^{-1}) to consistently yield a settling velocity to current shear velocity ratio < 1 , necessary to maintain sediment in suspension. For this fraction, the ratio of settling velocity to shear velocity was small enough (~ 0.1) to yield a relatively uniform distribution of sediment in the water column. Therefore, upper-water-column estimates of SSC are not much smaller than values obtained from measured turbidity 0.35 m above the bed at site 2.

Response to Increases in Sea Level and Storminess

An increase in mean water surface elevation in a tidal flat-marsh system will affect wave-generated bed shear stresses on the flat and marsh inundation frequency and duration.

Given strong westerly winds, maximum wave-generated bed shear stress on the tidal flat occurred at water surface elevations between MSL and MHHW (0.68 m above MSL at Wachapreague, VA), the range associated with stable marsh platforms (Fagherazzi and Wiberg 2009). For water surface elevations greater than MHHW, bottom shear stress declined (Fig. 5), consistent with the deepest-water bottom shear stress regime proposed by Fagherazzi and Wiberg (2009) for shallow bays.

Calculations of wave-generated shear stresses for a range of wind speeds and water depths show a similar pattern. For moderate fetch (10 km) and wind speeds (10 m s^{-1}), maximum wave-generated shear stresses on the tidal flat occur at a depth of 1.2 m (water surface elevation \sim MHHW), and decline at higher elevations (Fig. 12a). These conditions occurred together during less than 1% of all observations in 2013, but could occur more frequently and be less sensitive to wind direction with moderate sea-level rise. If marsh surface elevation keeps pace with steady SLR while tidal flat elevation remains constant, potential deposition (taken as proportional to the mass of sediment in water flooding the marsh), will continue to be maximized at a depth of 1.2 m above the tidal flat (now below MHHW). Thus while the depth of the water inundating the marsh during tidal flooding would remain the same as it is now, the sediment mass in the water flooding the marsh would decrease due to lower wave-generated shear stresses on the tidal flat because of the increase in water depth there. As a result, deposition rates would decline. However, if marsh and flat elevations remained constant (i.e., no vertical accretion) as sea level rises, potential deposition would increase for water depths above 1.2 m because, while SSC in the water flooding the marsh is slightly lower than maximum values, the mass of sediment in suspension and inundation time increase with increasing water depth above the marsh platform (Fig. 12b). This may increase the rate of deposition initially on bay-fronted marshes, but will eventually slow as the rate of accretion approaches the rate of SLR, similar to tidal creek marshes (D'Alpaos et al. 2011; Kirwan and Temmerman 2009). A third possibility that the marsh and tidal flat both change elevation at the rate of SLR would leave the system unchanged compared to the present but would require a net source of sediment sufficient to fill the bays at the rate of SLR.

Storms, taken here to mean high wind events, affect water surface elevations as well as wave heights in shallow coastal bays (Fagherazzi et al. 2010). The coincidence of high waves and higher-than-normal water levels should enhance rates of marsh deposition whereas high waves and lower-than-normal water levels should limit marsh deposition. Along the east coast of the US, strong northerly and easterly winds promote storm surge in shallow coastal bays while strong westerly or southwesterly winds tend to cause water surface elevations to drop (Fagherazzi et al. 2010). Therefore marshes with more

northerly and easterly exposure in shallow bays along this coast may experience higher deposition rates than marshes with more westerly or southwesterly exposure, such as our study site. These effects are likely to be particularly pronounced for microtidal marshes.

We examined wind records from 2009 to 2014 at the NOAA station at Kiptopeke, VA about 40 km S-SW of the study area, and compared them to water-levels from the NOAA station at Wachapreague, VA, about 16 km N-NE of the study area. [The Kiptopeke wind record is longer and in better agreement with other nearby wind records than the Wachapreague record (McLoughlin et al. 2015), while the Wachapreague tide record is very well correlated with water-level measurements in Hog Island Bay.] Winds from the SW-W ($210\text{--}300^\circ$), the direction of maximum fetch at our study site, were consistently associated with lower peak tidal elevations and water levels below predicted values compared to winds from the N-NE ($345\text{--}75^\circ$) during 2013 and the longer period 2009–2014. The difference is especially apparent for peak water levels $> 1.0 \text{ m}$ above MSL (highest predicted tide at Wachapreague) and winds $> 8 \text{ m s}^{-1}$, which occur on average about 4 times per year for winds from N-NE but only twice in 6 years for winds from SW-W (Table 3).

These results indicate that marsh orientation relative to dominant wind directions can be an important factor controlling deposition on bay-fronted marshes. Marshes oriented in the direction of surge-producing storm winds will likely be more affected by increases in storminess than marshes oriented in a direction where storm winds tend to decrease water levels. While increases or decreases in water level affect the whole system, marshes facing away from strong surge-

Table 3 Number of tidal cycles per year with high-tide water levels exceeding given surface elevations (relative to MSL) during 2013 and 2009–2014 for moderate–high wind speeds from SW-W and N-NE

2013				
Wind speed	High-tide elevation (marsh edge = 0.55 m above MSL)			
	0.4–0.6 m	0.6–0.8 m	0.8–1.0 m	> 1.0 m
SW-W				
8–12 m s^{-1}	2	1	1	0
> 12 m s^{-1}	0	0	0	0
N-NE				
8–12 m s^{-1}	3	7	4	4
> 12 m s^{-1}	0	0	0	1
2009–2014				
Wind speed	High-tide elevation			
	0.4–0.6 m	0.6–0.8 m	0.8–1.0 m	> 1.0 m
SW-W				
8–12 m s^{-1}	4	3.7	1.5	0.3
> 12 m s^{-1}	0.7	0.5	0.2	0
N-NE				
8–12 m s^{-1}	4	5.2	3	3.5
> 12 m s^{-1}	0.2	0.5	0.5	0.3

producing winds have little fetch for waves to develop from those storms. Instead, as is true of our study site, these marshes experience the highest waves during winds that lower water levels, thereby limiting the effectiveness of the highest winds for promoting deposition on the marsh surface even if they occur more frequently. Nevertheless, the highest SSC conditions in the upper water column over the tidal flat (site 2) were associated with northerly winds because even though the short fetch-limited wave size, these did produce the highest wave-driven bed shear stresses on the tidal flat during conditions when the marsh was inundated owing to a combination of spring tides and storm surge.

Implications for Modeling Deposition on Bay-Fronting Marshes

Most marsh deposition models were created for tidal channel marshes (e.g., Kirwan et al. 2010 and the models cited therein) where waves are not important. To model deposition on bay-fronted marshes, wave-driven resuspension, the primary control on SSC in the water flooding these marshes, must be accounted for. SSC over tidal flats adjacent to bay-fronted marshes can be calculated given sediment properties, water depth, and wave and current shear velocities (Appendix; Lawson et al. 2007; Mariotti et al. 2010). A number of studies (e.g., Mariotti et al. 2010; Carniello et al. 2011; Mariotti and Carr 2014; McLoughlin et al. 2015) have shown that the Young and Verhagen (1996a, b) parametric wave model provides good estimates of wave conditions in shallow water bodies given wind speed, fetch and water depth. These wave fields can be used to calculate wave-generated bed shear stresses on the tidal flats (Wiberg and Sherwood 2008). Owing to the generally regular nature of tides, characteristic tidal current shear velocities can be obtained from a time series of currents spanning a typical spring-neap cycle or from a hydrodynamic model that resolves tidal time scales.

The general correspondence between SSC in the upper water column over the tidal flat and over the marsh edge (Fig. 9c, d) supports an approach to modeling flat-marsh sediment exchange like that used by Mariotti and Carr (2014) and Carr et al. (2018) in which the flux between the flat and the marsh is calculated assuming a tidal dispersion mechanism driven by differences in SSC over the flat and over the marsh (initially 0 for a vegetated marsh) and depends on tidal range and marsh elevation. Our results indicate, however, that meteorological effects on water-surface elevation and the timing of wind events relative to spring-neap cycles must be accounted for in addition to tidal range for microtidal marshes that primarily flood during spring tides and storm surge.

Our study site provides a useful example of the importance of accounting for meteorological effects on water surface elevations in microtidal bays. If the study marsh only flooded when predicted tidal levels exceeded the elevation of the

marsh platform (accounting for spring-neap variations but not storm surge), inundation frequency would decrease from 17% to 9% of the record and mean inundation depth would decrease from 0.18 m to 0.13 m during N13; for M14, inundation frequency would decrease from 19 to 11% of the record and mean inundation depth would decrease from 0.20 to 0.10 m. As a result, predicted deposition would be at least a factor of two lower. Similarly, if high winds that suppressed water surface elevations occurred when a marsh would otherwise be expected to flood, deposition would be overestimated. Accounting for meteorological effects of water surface elevations could be one of the more challenging aspects of modeling deposition on microtidal marshes, and affects tidal creek marshes (e.g., Christiansen 1998) as well as bay-fronted marshes. Long-term records of coincident winds and water levels (e.g., Table 3) are likely the best basis for characterizing the conditions associated with water surface elevations that are higher or lower than expected due to tides alone.

An additional challenge of modeling deposition on bay-fronted marshes is the lack of stability of the marsh edge itself (Mariotti and Fagherazzi 2013). In the VCR and many other coastal bay systems (e.g., Lagoon of Venice; Marani et al. 2011), marshes are retreating along their boundary with the bay. This retreat changes the spatial relationship between earlier deposits and the marsh edge. For example, at our study site on Chimney Pole marsh, the marsh edge has been retreating at an average rate of 1.5–2.0 m year⁻¹ (McLoughlin et al. 2015). As a result, deposits formerly 8 m from the marsh edge (the location on maximum deposition in our study) would be at the marsh edge within 5 years. The fate of the sediment released during marsh-edge retreat is uncertain, likely moving along the edge when water surface elevations are below the level of the marsh platform and potentially providing a supply of sediment to the marsh when the marsh is flooded. More detailed morphodynamic modeling and measurements are needed to resolve this important question.

Conclusions

Marshes bordering shallow coastal bays are eroding in many regions of the world, and contribute to marsh loss even when interior marshland is stable (Mariotti and Fagherazzi 2013; Fagherazzi 2013), yet little is known about how sediment is transported across bay-fronted marshes, making their response to sea level rise and increased storminess poorly understood. Sediment transport near bay-fronted marshes is fundamentally different than near tidal creek marshes owing to the presence of wind-driven waves and currents. Wave events in shallow coastal bays are predominantly responsible for elevating suspended sediment concentrations over tidal flats. In contrast to marshes bordering tidal creeks, tides are relatively unimportant in controlling the concentration of sediment in

water flooding bay-fronted marshes. The direction of surface currents can be variable during times when water elevations are high enough to flood the marsh, but our results show that sediment in the upper water column over the tidal flat adjacent to a marsh is effectively transported across the marsh edge when the marsh floods.

While wind-driven waves control suspended sediment concentrations over the tidal flats, we found that the largest resuspension events typically do not enhance sediment fluxes onto the westward facing marshes of our study area owing to a lack of correlation between wind conditions suitable for wave generation and tidal water levels above the elevation of the marsh platform. In contrast, north-northeast facing marshes may benefit from Nor'easters that bring both high winds and storm surge (Fagherazzi et al. 2010). Therefore, marsh-edge orientation relative to the wind direction associated with maximum fetch, as well as the long-term relationship between wind conditions and deviations from expected tidal water levels, can be important factors controlling sediment deposition on bay-fronted marshes in microtidal systems.

The presence of waves during periods of marsh flooding alters the pattern of sediment deposition on marshes bordering bays, preventing deposition near the edge and displacing maximum deposition inland. As a result, whereas the marsh fringe bordering tidal creeks experiences the highest local deposition rates, the marsh fringe bordering open water is non-depositional or even erosional. An increase in sea level relative to marsh platform elevation will increase flooding frequency and the mass of wave-driven suspended sediment transported onto the marsh even if water depths over the tidal flat exceed the depth associated with maximum near-surface SSC. This will initially enhance sediment deposition on the marsh if sea level rises relative to marsh elevation. However, deeper water over the tidal flats coupled with a constant marsh flooding frequency (marsh elevation and sea-level rising in step) will ultimately lead to a reduction in sediment fluxes from tidal flats to adjacent marshes.

Acknowledgements Primary support for this research was provided by the National Science Foundation through the VCR LTER award 1237733. Additional support was provided by NSF OCE-SEES award 1426981 and NSF EAR-GLD award 1529245. Logistical support was provided by the staff and facilities at the Anheuser-Busch Coastal Research Center. Comments from two anonymous reviewers helped to improve the manuscript.

Appendix

Current-generated bed shear stress, τ_{curr} , was calculated using the expression:

$$\tau_{curr} = C_D \rho u^2$$

where $\rho = 1020 \text{ kg m}^{-3}$ is water density, u is current speed, and C_D is the drag coefficient, estimated as:

$$C_D = gn^2 / (h^{1/3})$$

where n is the roughness coefficient

$$n = \left[\frac{\sqrt{8g}}{h^{1/6}} \left(2 \log_{10} \left(\frac{h}{D_{84}} \right) + 1 \right) \right]^{-1}$$

(Homberger et al. 2014; Lawson et al. 2007), h is water depth, $g = 9.81 \text{ m s}^{-2}$, and D_{84} is the 84th percentile of the grain size distribution.

Wave-induced bottom orbital velocity, u_b , was calculated as:

$$u_b = \frac{\pi H_s}{T \sinh(kh)}$$

(Wiberg and Sherwood 2008) and wave-generated bed shear stress, τ_{wave} , was estimated as:

$$\tau_{wave} = 0.5 f_w \rho u_b^2$$

where

$$f_w = 0.04 \left(\frac{u_b T}{2\pi k_s} \right)^{-0.25}$$

(Fredsoe and Deigaard 1992), H_s is significant wave height, T is wave period, k is wave number ($2\pi/L$), L is wave length, f_w is the wave friction factor, and $k_s = 3D_{84}$ is the roughness length scale of the bed. Total bed shear stress was calculated as the sum of wave and current shear stress.

To estimate suspended sediment concentrations, C_s , throughout the full water column, the Rouse equation (Rouse 1937) was applied using 3 grain-size fractions ($7 \mu\text{m}$ ($w_{si} = 3 \times 10^{-5} \text{ m s}^{-1}$); $25 \mu\text{m}$ ($w_{si} = 4 \times 10^{-4} \text{ m s}^{-1}$); $100 \mu\text{m}$ ($w_{si} = 0.005 \text{ m s}^{-1}$))

$$C_{si} = C_a \left(\frac{z \times (h - z_a)}{z \times (h - z)} \right)^{r_i}$$

where $r_i = -w_{si}/(\kappa u_{*curr})$ is the Rouse parameter for each grain size fraction, i , w_{si} is the particle settling velocity for each size fraction, u_{*curr} is current shear velocity, κ is von Karman's constant (0.41), and z is the height in the water column at which C_{si} is being estimated. C_a is the reference concentration at the reference height at the level z_a . When turbidity measurements are available, C_a is taken as the suspended sediment concentration estimated from measured turbidity and z_a is the height of the turbidity sensor. When turbidity measurements are not available, we estimated C_a as

$$C_a = C_{bed} \frac{\gamma S}{1 + \gamma S}$$

(Smith and McLean 1977), where $S = (\tau_b - \tau_{cr})/\tau_{cr}$ is the excess shear stress determined from τ_b , the total bed shear stress exerted by waves and currents, $z_a = 3D_{50}$, D_{50} is the median grain size, and $C_{bed} = 0.3$ is the concentration of sediment in the bed ($1.0 - \text{porosity}$), consistent with a muddy bed (Wheatcroft et al. 2007). Critical shear stress was determined to be $\tau_{cr} = 0.07$ Pa from a plot of NTU versus total shear stress at site 2 (Online Resource 2). This agrees with values based on erosion rate measurements from Lawson (2004). We set the value of the resuspension coefficient $\gamma = 5e^{-4}$, by scaling the estimated SSC to match the measured SSC. Field and laboratory studies have shown large variation in values of γ , ranging from 10^{-2} to 10^{-5} (e.g., Smith and McLean 1977; Wiberg and Smith 1983; Sternberg et al. 1986; Hill et al. 1988; Drake and Cacchione 1989).

References

- Beckman Coulter. 2011. *Instructions for use: LS 13 320 laser diffraction particle size analyzer, PN B05577AB, revision 10/11*. California: Brea.
- Butzeck, C., A. Eschenbach, A. Grönröft, et al. 2015. Sediment deposition and accretion rates in tidal marshes are highly variable along estuarine salinity and flooding gradients. *Estuaries and Coasts* 38: 434. <https://doi.org/10.1007/s12237-014-9848-8>.
- Cahoon, D.R., and D.J. Reed. 1995. Relationships among marsh surface topography, hydroperiod, and soil accretion in a deteriorating Louisiana salt marsh. *Journal of Coastal Research* 11 (2): 357–369.
- Callaghan, D.P., T.J. Bouma, P. Klaassen, D. van der Wal, M.J.F. Stive, and P.M.J. Herman. 2010. Hydrodynamic forcing on salt-marsh development: Distinguishing the relative importance of waves and tidal flows. *Estuarine, Coastal, & Shelf Science* 89: 73–88.
- Carniello, L., A. D'Alpaos, and A. Defina. 2011. Modeling wind waves and tidal flows in shallow micro-tidal basins. *Estuarine, Coastal, & Shelf Science* 92: 263–276.
- Carniello, L., A. Defina, and A. D'Alpaos. 2012. Modeling sand-mud transport induced by tidal currents and wind-waves in shallow microtidal basins: Application to the Venice Lagoon (Italy). *Estuarine, Coastal & Shelf Science* 102-3: 105–115.
- Carr, J., Mariotti, G., Fagherazzi, S., McGlathery, K., and P. Wiberg. 2018. Exploring the impacts of seagrass on coupled marsh-tidal flat morphodynamics. *Frontiers in Environmental Science* 6: 92.
- Castagno, K.A., A.M. Jiménez-Robles, J.P. Donnelly, P.L. Wiberg, M.S. Fenster, S. Fagherazzi. (2018). Intense storms increase the stability of tidal bays. *Geophysical Research Letters*.
- Christiansen, T. 1998. Sediment deposition on a tidal salt marsh. (unpublished PhD dissertation). In *University of Virginia*. Charlottesville: USA.
- Christiansen, T., P.L. Wiberg, and T.G. Mulligan. 2000. Flow and sediment transport on a tidal salt marsh surface. *Estuarine, Coastal and Shelf Science* 50: 315–331.
- D'Alpaos, A., S.M. Mudd, and L. Carniello. 2011. Dynamic response of marshes to perturbations in suspended sediment concentrations and rates of relative sea level rise. *Journal of Geophysical Research* 116: F04020. <https://doi.org/10.1029/2011JF002093>.
- Deaton, C.D., C.J. Hein, and M.L. Kirwan. 2017. Barrier island migration dominates ecogeomorphic feedbacks and drives salt marsh loss along the Virginia Atlantic Coast, USA. *Geology* 45 (2): 123–126. <https://doi.org/10.1130/G38459.1>.
- Dietrich, W.E. 1982. Settling velocity of natural particles. *Water Resources Research* 18: 1615–1626.
- Donelan, M.A., J. Hamilton, and W.H. Hui. 1985. Directional spectra for wind-generated waves. *Philosophical Transactions of the Royal Society of London, A A* 315L: 509–562.
- Drake, D.E., and D.A. Cacchione. 1989. Estimates of the suspended sediment reference concentration (C_α) and resuspension coefficient (γ_0) from near-bottom observations on the California shelf. *Continental Shelf Research* 9: 51–64.
- Duvall, M.S. 2014. The effects of waves and tidal inundation on sediment flux and deposition across a bay-marsh boundary. (unpublished Master's thesis). In *University of Virginia*. Charlottesville: USA.
- Ensign, S.H., and C. Currin. 2017. Geomorphic implications of particle movement by water surface tension in a salt marsh. *Wetlands* 37 (2): 245–256.
- Fagherazzi, S. 2013. The ephemeral life of a salt marsh. *Geology* 41 (8): 943–944. <https://doi.org/10.1130/focus082013.1>.
- Fagherazzi, S., and P.L. Wiberg. 2009. Importance of wind conditions, fetch, and water levels on wave-generated shear stresses in shallow intertidal basins. *Journal of Geophysical Research* 114: F03022.
- Fagherazzi, S., G. Mariotti, J.H. Porter, K.J. McGlathery, and P.L. Wiberg. 2010. Wave energy asymmetry in shallow bays. *Geophysical Research Letters* 37: L24601. <https://doi.org/10.1029/2010GL045254>.
- Fagherazzi, S., P.L. Wiberg, S. Temmerman, E. Struyf, Y. Zhao, and P.A. Raymond. 2013. Fluxes of water, sediment, and biogeochemical compounds in salt marshes. *Ecological Processes* 2: 3.
- Fredsoe, J., and R. Deigaard. 1992. *Mechanics of Coastal Sediment Transport. Advanced Series on Ocean Engineering Vol. 3*. Singapore: World Science.
- French, J.R., and T. Spencer. 1993. Dynamics of sedimentation in a tide-dominated backbarrier saltmarsh, Norfolk, UK. *Marine Geology* 110 (3–4): 315–331.
- Friedrichs, C.T., and J.E. Perry. 2001. Tidal salt marsh morphodynamics. *Journal of Coastal Research* 27: 6–36.
- Ganju, N.K., M.L. Kirwan, P.J. Dickhudt, G.R. Guntenspergen, D.R. Cahoon, and K.D. Kroeger. 2015. Sediment transport-based metrics of wetland stability. *Geophysical Research Letters* 42: 7992–8000. <https://doi.org/10.1002/2015GL065980>.
- Ganju, N.K., Z. Defne, M.L. Kirwan, S. Fagherazzi, A. D'Alpaos, and L. Carniello. 2017. Spatially integrative metrics reveal hidden vulnerability of microtidal salt marshes. *Nature Communications* 8: 14156. <https://doi.org/10.1038/ncomms14156>.
- Gompertz, B. 1825. On the nature of the function expressive of the law of human mortality, and on a new mode of determining the value of life contingencies. *Philosophical Transactions of the Royal Society of London* 115: 513–585. <https://doi.org/10.1098/rstl.1825.0026>.
- Hansen, J.C.R., and M.A. Reidenbach. 2012. Wave and tidally driven flows in eelgrass beds and their effect on sediment suspension. *Marine Ecology Progress Series* 448: 271–287. <https://doi.org/10.3354/meps09225>.
- Hill, P.S., A.R.M. Nowell, and P.A. Jumars. 1988. Flume evaluation of the relationship between suspended sediment concentration and excess boundary shear stress. *Journal of Geophysical Research* 93: 12499–12510.
- Hornberger, G.M., P.L. Wiberg, J.P. Raffensperger & P. D'Odorico. 2014. Elements of physical hydrology, 2nd edition. Johns Hopkins press.
- Kastler, J., and P. Wiberg. 1996. Sedimentation and boundary changes of Virginia salt marshes. *Estuarine, Coastal and Shelf Science* 42: 683–700.
- Keamey, M.S., and R.E. Turner. 2016. Can these widespread and fragile marshes survive increasing climate–sea level variability and human action? *Journal of Coastal Research* 32 (3): 686–699.
- Kirwan, M., and S. Temmerman. 2009. Coastal marsh response to historical and future sea-level acceleration. *Quaternary Science Reviews* 28: 1801–1808. <https://doi.org/10.1016/j.quascirev.2009.02.022>.

- Kirwan, M.L., G.R. Guntenspergen, A. D'Alpaos, J.T. Morris, S.M. Mudd, and S. Temmerman. 2010. Limits on the adaptability of coastal marshes to rising sea level. *Geophysical Research Letters* 37: L23401.
- Kirwan, M.L., D.C. Walters, W.G. Reay, and J.A. Carr. 2016. Sea level driven marsh expansion in a coupled model of marsh erosion and migration. *Geophysical Research Letters* 43: 4366–4373. <https://doi.org/10.1002/2016GL068507>.
- Lawson, S. E. (2004). *Sediment suspension as a control on light availability in a coastal lagoon*. (Unpublished Master's Thesis). Charlottesville, VA: University of Virginia.
- Lawson, S.E., P.L. Wiberg, K.J. McGlathery, and D.C. Fugate. 2007. Wind-driven sediment suspension controls light availability in shallow coastal lagoon. *Estuaries and Coasts* 30 (1): 102–112.
- Leonard, L.A. 1997. Controls of sediment transport and deposition in an incised mainland marsh basin, southeastern North Carolina. *Wetlands* 17 (2): 263–274.
- Leonard, L.A., and M.E. Luther. 1995. Flow hydrodynamics in tidal marsh canopies. *Limnology and Oceanography* 40 (8): 1474–1484.
- Leonardi, N., N.K. Ganju, and S. Fagherazzi. 2016. A linear relationship between wave power and erosion determines salt-marsh resilience to violent storms and hurricanes. *Proceedings of the National Academy of Sciences* 113: 64–68.
- Lynch, J.C., Hensel, P., and D.R. Cahoon. 2015. *The surface elevation table and marker horizon technique: A protocol for monitoring wetland elevation dynamics*. *Natural Resource Report NPS/NCBN/NRR-2015/1078*. Fort Collins, CO: National Park Service.
- Marani, M., A. D'Alpaos, S. Lanzoni, and M. Santalucia. 2011. Understanding and predicting wave erosion of marsh edges. *Geophysical Research Letters* 38: L21401. <https://doi.org/10.1029/2011GL048995>.
- Mariotti, G., and J. Carr. 2014. Dual role of salt marsh retreat: Long-term loss and short-term resilience. *Water Resources Research* 50: 2963–2974.
- Mariotti, G., and S. Fagherazzi. 2010. A numerical model for the coupled long-term evolution of salt marshes and tidal flats. *Journal of Geophysical Research* 115: F01004.
- Mariotti, G., and S. Fagherazzi. 2013. Critical width of tidal flats triggers marsh collapse in the absence of sea-level rise. *Proceedings of the National Academy of Sciences USA* 110 (14): 5353–5356.
- Mariotti, G., S. Fagherazzi, P.L. Wiberg, K.J. McGlathery, L. Carniello, and A. Defina. 2010. Influence of storm surges and sea level on shallow tidal basin erosive processes. *Journal of Geophysical Research* 115: C11012.
- McLoughlin, S.M. (2010). *Erosional processes along salt marsh edges on the eastern shore of Virginia*. (unpublished Master's thesis). Charlottesville, VA, USA: University of Virginia.
- McLoughlin, S.M., P.L. Wiberg, I. Safak, and K.J. McGlathery. 2015. Rates and forcing of marsh-edge erosion in a shallow coastal bay: Virginia. *Estuaries and Coasts*. <https://doi.org/10.1007/s12237-014-9841-2>.
- Möller, I., T. Spencer, and J.R. French. 1996. Wind wave attenuation over saltmarsh surfaces: Preliminary results from Norfolk, England. *Journal of Coastal Research* 12 (4): 1009–1016.
- Möller, I., T. Spencer, J.R. French, D.J. Leggett, and M. Dixon. 1999. Wave transformation over salt marshes: A field and numerical modeling study from North Norfolk, England. *Estuarine, Coastal & Shelf Science* 49 (3): 411–426.
- Möller, I., M. Kudella, F. Rupprecht, T. Spencer, M. Paul, B.K. van Wesenbeeck, G. Wolters, K. Jensen, T.J. Bouma, M. Miranda-Lange, and S. Schimmels. 2014. Wave attenuation over coastal salt marshes under storm surge conditions. *Nature Geoscience* 7: 727–731. <https://doi.org/10.1038/ngeo2251>.
- Morris, J.T., P.V. Sundareshwar, C.T. Nietch, B. Kjerfve, and D.R. Cahoon. 2002. Responses of coastal wetlands to rising sea level. *Ecology* 83: 2869–2877.
- Nepf, H.M. 1999. Drag, turbulence, and diffusion in flow through emergent vegetation. *Water Resources Research* 35 (2): 479–489. <https://doi.org/10.1029/1998WR900069>.
- Oertel, G.F. 2001. Hypsographic, hydro-hypsographic, and hydrological analysis of coastal bay environments, Great Machipongo Bay, Virginia. *Journal of Coastal Research* 17: 775–783.
- Paramor, O.A.L., and R.G. Hughes. 2004. The effects of bioturbation and herbivory by the polychaete *Nereis diversicolor* on loss of saltmarsh in south-east England. *Journal of Applied Ecology* 41: 449–463.
- Pasternack, G.B., and G.S. Brush. 1998. Sedimentation cycles in a river-mouth tidal freshwater marsh. *Estuaries* 21: 407–415. <https://doi.org/10.2307/1352839>.
- Pestrong, R. 1969. The shear stress of tidal marsh sediments. *Journal of Sedimentary Petrology* 39: 322–326.
- Pratolongo, P., G.M.E. Perillo, and M.C. Piccolo. 2010. Combined effects of waves and plants on a mud deposition event at a mudflat-saltmarsh edge in the Bahía Blanca estuary. *Estuarine Coastal & Shelf Science* 87: 207–212. <https://doi.org/10.1016/j.ecss.2009.09.024>.
- Prietas, A.M., G. Mariotti, N. Leonardi, and S. Fagherazzi. 2010. Coupled wave energy and erosion dynamics along a salt marsh boundary, Hog Island Bay, Virginia, USA. *Journal of Marine Science and Engineering* 3 (3): 1041–1065.
- Reidenbach, M., Timmerman, R. (2014). *Wind speed and direction on Godwin Island, 2013–2014* [data file]. Retrieved from <https://doi.org/10.6073/pasta/0d07604a03d09e327abbe2b81e44ac11>
- Rouse, H. 1937. Modern conceptions of the mechanics of turbulence. *Transactions of the American Society of Civil Engineers* 102: 436–505.
- Schuerch, M., A. Vafeidis, T. Slawig, and S. Temmerman. 2013. Modeling the influence of changing storm patterns on the ability of a salt marsh to keep pace with sea level rise. *Journal of Geophysical Research* 118: 84–96. <https://doi.org/10.1029/2012JF002471>.
- Smith, J.D., and S.R. Mclean. 1977. Spatially averaged flow over a wavy surface. *Journal of Geophysical Research* 82: 1735–1746.
- Sternberg, R.W., D.A. Cacchione, D.E. Drake, and K. Kranck. 1986. Suspended sediment dynamics in an estuarine tidal channel within San Francisco Bay, California. *Marine Geology* 71: 237–258.
- Temmerman, S., G. Govers, S. Wartel, and P. Meire. 2003. Spatial and temporal factors controlling short-term sedimentation in a salt and freshwater tidal marsh, Scheldt estuary, Belgium, SW Netherlands. *Earth Surface Processes & Landforms* 28: 739–755. <https://doi.org/10.1002/esp.495>.
- Tonelli, M., S. Fagherazzi, and M. Petti. 2010. Modeling wave impact on salt marsh boundaries. *Journal of Geophysical Research* 115: C09028.
- Wheatcroft, R.A., P.L. Wiberg, et al. 2007. Post-depositional alteration of strata. In *Continental margin sedimentation: Transport to sequence*, ed. C. Nittrouer et al., 101–155. Oxford: Blackwell Pub.
- Wiberg, P.L. 2016. *Evolution of a marsh as the bay-marsh boundary "front" moves through it*. Abstract EP21B-0879 presented at the 2016 fall meeting, 12–16. San Francisco: AGU.
- Wiberg, P.L., and C.R. Sherwood. 2008. Calculating wave-generated bottom orbital velocities from surface-wave parameters. *Computers & Geosciences* 34: 1243–1262.
- Wiberg, P.L., and J.D. Smith. 1983. A comparison of field data and theoretical models for wave-current interactions at the bed on the continental shelf. *Continental Shelf Research* 2: 147–162.
- Wiberg, P.L., B.A. Law, R.A. Wheatcroft, T.G. Milligan, and P.S. Hill. 2013. Seasonal variations in erodibility and sediment transport potential in a mesotidal channel-flat complex, Willapa Bay, WA.

- Continental Shelf Research* 60: S185–S197. <https://doi.org/10.1016/j.csr.2012.07.021>.
- Wiberg, P.L., J.A. Carr, I. Safak, and A. Anutaliya. 2015. Quantifying the distribution and influence of non-uniform bed properties in shallow coastal bays. *Limnology & Oceanography Methods* 13: 746–762. <https://doi.org/10.1002/lom3.10063>.
- Widdows, J., N.D. Pope, and M.D. Brinsley. 2008. Effect of *Spartina anglica* stems on near-bed hydrodynamics, sediment erodibility and morphological changes on an intertidal mudflat. *Marine Ecological Progress Series* 362: 45–57.
- Wilson, C.A., Z.J. Hughes, and D.M. FitzGerald. 2012. The effects of crab bioturbation on Mid-Atlantic saltmarsh tidal creek extension: Geotechnical and geochemical changes. *Estuarine, Coastal and Shelf Science* 106: 33–44.
- Wunsch, C., and D. Stammer. 1997. Atmospheric loading and the oceanic “inverted barometer” effect. *Reviews of Geophysics* 35: 79–107.
- Young, I.R., and L.A. Verhagen. 1996a. The growth of fetch limited waves in water of finite depth. 1. Total energy and peak frequency. *Coastal Engineering* 29 (1–2): 47–78.
- Young, I.R., and L.A. Verhagen. 1996b. The growth of fetch limited waves in water of finite depth. 2. Spectral evolution. *Coastal Engineering* 29 (1–2): 79–99.